The Origin of Physiological Local mGluR1 Supralinear Ca 2+ Signals in Cerebellar Purkinje Neurons

Karima Ait Ouares, Marco Canepari

In press

The origin of physiological local mGluR1 supralinear Ca^{2+} signals in cerebellar Purkinje neurons

Running title: *mGluR1 supralinear Ca^{2+} signal in Purkinje neurons*

Karima Ait Ouares[1,2], **Marco Canepari**[1,2,3,*]

[1]Univ. Grenoble Alpes, CNRS, LIPhy, F-38000 Grenoble, France. [2]Laboratories of Excellence, Ion Channel Science and Therapeutics, France. [3]Institut National de la Santé et Recherche Médicale, France.

Address of the submitting and corresponding author: Marco Canepari, Laboratoire Interdisciplinaire de Physique (UMR 5588), Bat. E45, 140 avenue de la physique, Domaine univ., 38402 St Martin d'Hères cedex, France. Email: marco.canepari@univ-grenoble-alpes.fr

Number of pages: 28. Number of figures: 13.
Number of words for abstract (250), introduction (643), discussion (1436)

Conflict of interests: *None*

Acknowledgements: This work was supported by the *Agence Nationale de la Recherche* through three grants (ANR-14-CE17-0006 - WaveFrontImag; Labex *Ion Channels Science and Therapeutics:* program number ANR-11-LABX-0015 and National Infrastructure France Life Imaging “Noeud Grenoblois”) and by the *Federation pour la recherché sur le Cerveau* (FRC – Grant *Espoir en tête*, Rotary France). We thank Dr. Boris Barbour for useful discussions during the project, for reading the manuscript before submission and for advices on improving the clarity of the figures.

Author contributions: K.AO. conducted the experiments; M.C. designed the experiments and wrote the paper.

Abstract

In mouse cerebellar Purkinje neurons (PNs), the climbing fibre (CF) input provides a signal to parallel fibre (PF) synapses triggering PF synaptic plasticity. This signal is given by supralinear Ca^{2+} transients, associated with the CF synaptic potential and co-localised with the PF Ca^{2+} influx, occurring only when PF activity precedes the CF input. Here, we unravel the biophysical determinants of supralinear Ca^{2+} signals associated with paired PF-CF synaptic activity. We used membrane potential (V_m) and Ca^{2+} imaging to investigate the local CF-associated Ca^{2+} influx following a train of PF synaptic potentials, in two cases: 1. when the dendritic V_m is hyperpolarised below the resting V_m; and 2. when the dendritic V_m is at rest. We found that supralinear Ca^{2+} signals are mediated by type-1 metabotropic glutamate receptors (mGluR1s) when the CF input is delayed by 100-150 ms from the first PF input in both cases. When the dendrite is hyperpolarised only, however, mGluR1s boost neighbouring T-type channels providing a mechanism for local coincident detection of PF-CF activity. The resulting Ca^{2+} elevation is locally amplified by saturation of endogenous Ca^{2+} buffers produced by the PF-associated Ca^{2+} influx *via* the mGluR1-mediated non selective cation conductance. In contrast, when the dendritic V_m is at rest, mGluR1s increase dendritic excitability by inactivating A-type K^+ channels, but this phenomenon is not restricted to the activated PF synapses. Thus, V_m is likely a crucial parameter in determining PF synaptic plasticity and the occurrence of hyperpolarisation episodes is expected to play an important role in motor learning.

Significance statement

In Purkinje neurons, parallel fibre synaptic plasticity, determined by coincident activation of the climbing fibre input, underlies cerebellar learning. We unravel the biophysical mechanisms allowing the CF input to produce a local Ca^{2+} signal exclusively at the sites of activated parallel fibres. We show that when the membrane potential is hyperpolarised with respect to the resting membrane potential type-1 metabotropic glutamate receptors locally enhance Ca^{2+} influx mediated by T-type Ca^{2+} channels and that this signal is amplified by saturation of endogenous buffer also mediated by the same receptors. The combination of these two mechanisms is therefore capable of producing a Ca^{2+} signal at the activated parallel fibre sites, suggesting a role of Purkinje neuron membrane potential in cerebellar learning.

Introduction

In cerebellar Purkinje neurons (PNs), short- and long-term synaptic plasticity of the parallel fibre (PF) inputs can be induced by pairing PF excitatory synaptic potentials (EPSPs) with a climbing fibre (CF) EPSP (Wang et al., 2000; Brenowitz and Regehr, 2005; Safo and Regehr, 2005). These forms of plasticity, that are believed to underlie associative motor learning and control behaviours (Ito, 2001), are homosynaptic and they require local Ca^{2+} elevation at the site of activated PF synapses. Precisely, the Ca^{2+} transient triggered by a CF-EPSP alone is not local (Knöpfel et al., 1991; Miyakawa et al., 1992; Canepari and Vogt, 2008; Ait Ouares et al., 2019) since it is caused by a depolarising transient, originating in the soma and in the initial dendritic segment, that spreads to distal dendrites to open voltage-gated Ca^{2+} channels (VGCCs). When a CF-EPSP occurs after PF activity, the associated Ca^{2+} transient is larger than the summation of the two Ca^{2+} transients triggered by PF and CF inputs alone, and it is therefore referred as "supralinear" Ca^{2+} signal (Brenowitz and Regehr, 2005). However, in contrast to the Ca^{2+} transient associated with an unpaired CF-EPSP, the supralinear Ca^{2+} signal associated with paired PF and CF inputs is localised exclusively at the site of activated PF synapses.

The ability of a spread physiological signal to trigger a local signal, in combination with synaptic activity, exclusively at the sites of activated synapse, is a crucial requirement for coincident detection and associative plasticity in many systems. In hippocampal and neocortical pyramidal neurons, synchronous action potentials and excitatory synaptic activity can potentiate activated synapses (Debanne, 2001). In this case, action potentials transiently depolarising the dendrites can provide a signal localised at activated synapses by unblocking NMDA receptors from Mg^{2+} (Ascher and Nowak, 1987). In the case of PF synaptic plasticity induced by coincident CF inputs, however, the underlying biophysical mechanism does not involve NMDA receptors but instead type-1 metabotropic glutamate receptors (mGluR1s) which are locally activated by glutamate release from PF terminals (Hartell, 1994; Wang et al., 2000; Brenowitz and Regehr, 2005; Safo and Regehr, 2005). Since mGluR1 activation is not voltage-dependent, the fundamental question is to understand how a CF-EPSP, that alone generates a depolarisation and a Ca^{2+} influx everywhere in the dendrite, can trigger a strong localised Ca^{2+} elevation, in combination with mGluR1 activation, exclusively at the site of activated PFs.

In a recent study, we have demonstrated that the dendritic depolarisation produced by a CF-EPSP activates two types of VGCCs, namely T-type and P/Q-type VGCCs, and that the activation of both channels is determined by the dendritic membrane potential (V_m) at the beginning of the CF-EPSP (Ait Ouares et al., 2019). Specifically, at initial hyperpolarised V_m, the dendritic Ca^{2+} transient is largely mediated by T-type VGCCs while activation of A-type voltage-gated K^+ channels limits the opening of P/Q-type VGCCs. In contrast, at initial depolarised V_m, T and A channels are inactivated and the larger dendritic depolarising transient activates P/Q-type VGCCs that mediate Ca^{2+} spikes. It was also shown that both T-type VGCCs (Hildebrand et al., 2009; Isope et al., 2012) and P/Q-type VGCCs (Otsu et al., 2014) can be boosted by mGluR1 activation, providing two potential biophysical mechanisms underlying localised supralinear Ca^{2+} signals that are required for coincident detection and PF synaptic plasticity.

In the present study we addressed the question of how a CF-EPSP can generate a supralinear Ca^{2+} signal exclusively at the sites of activated PF synapses. We used a protocol of moderate PF stimulation

mimicking a physiological burst to reveal the biophysical mechanism that permit a CF-EPSP to trigger a localised signal at the site of activated PF synapses in realistic scenarios. We used ultrafast V_m and Ca^{2+} imaging, using indicators of different affinity and a series of selective pharmacological manipulations and we performed a detailed analysis to elucidate the different mechanisms underlying supralinear Ca^{2+} signals under different conditions.

Materials and methods

SLICE PREPARATION, SOLUTIONS, ELECTROPHYSIOLOGY AND PHARMACOLOGY

Experiments were ethically carried out in accordance with European Directives 2010/63/UE on the care, welfare and treatment of animals. Procedures were reviewed by the ethics committee affiliated to the animal facility of the university (D3842110001). We used 21-35 postnatal days old mice (C57BL/6j) of either sex. Animals were anesthetised by isofluorane inhalation and the entire cerebellum was removed after decapitation. Cerebellar sagittal slices (250 µm thick) were prepared following established procedures (Vogt et al., 2011a; Vogt et al., 2011b; Ait Ouares et al., 2016) using a Leica VT1200 (Leica, Wetzlar, Germany). Slices were incubated at 37°C for 45 minutes before use. The extracellular solution contained (in mM): 125 NaCl, 26 $NaHCO_3$, 1 $MgSO_4$, 3 KCl, 1 NaH_2PO_4, 2 $CaCl_2$ and 20 glucose, bubbled with 95% O_2 and 5% CO_2. The intracellular solution contained (in mM): 125 $KMeSO_4$, 5 KCl, 8 $MgSO_4$, 5 Na_2-ATP, 0.3 Tris-GTP, 12 Tris-Phosphocreatine, 20 HEPES, adjusted to pH 7.35 with KOH. In V_m imaging experiments, PNs were loaded with the voltage-sensitive dye (VSD) JPW1114 as previously described (Canepari and Vogt, 2008) and in some experiments also with the Ca^{2+} indicator Fura-2FF (at 1 mM) using a previously described procedure (Vogt et al., 2011a). In experiments of Ca^{2+} imaging only, Oregon Green BAPTA-5N (OG5N) was added to the internal solution at 2 mM concentration and, in some experiments, also Fura-2 (Fura2) at 0.4 mM concentration was included. Patch-clamp recordings were made at 32-34°C using a Multiclamp amplifier 700A (Molecular Devices, Sunnyvale, CA) and electrical signals were acquired at 20 kHz using the A/D board of the CCD camera, regardless of the imaging acquisition rate. The measured V_m was corrected for junction potential (-11 mV) as previously estimated (Canepari et al., 2010). PF- and CF-EPSPs were elicited by current pulses of 5-20 µA amplitude and 100 µs duration delivered by separate electrodes. To avoid jitters, the stimulation protocols were precisely controlled with a Master-8 pulse generator (A.M.P.I., Jerusalem, Israel). All recordings were performed at least 30 minutes after establishing whole cell. This minimum time before starting recording was 45 minutes in experiments with Fura2, heparin and ryanodine. In V_m imaging experiments, cells were initially loaded with the voltage sensitive dye JPW1114 and re-patched with a solution without this dye to avoid toxicity due to dye overloading. 7-(Hydroxyimino)cyclopropa[*b*]chromen-1a-carboxylate ethyl ester (CPCCOEt), (1*S*,2*S*)-2-[2-[[3-(1*H*-Benzimidazol-2-yl)propyl]methylamino]ethyl]-6-fluoro-1,2,3,4-tetrahydro-1-(1-methylethyl)-2-naphthalenyl-cyclopropanecarboxylate-dihydrochloride (NNC550396 or NNC) and *N*,*N*,*N*-Trimethyl-5-[(tricyclo[3.3.1.$1^{3,7}$]dec-1-ylmethyl)amino]-1-pentanaminium bromide hydrobromide (IEM1460) were dissolved in exracellular solution and applied to the bath *via* the perfusion system. Heparin sodium salt, 1*H*-Pyrrole-2-carboxylic acid (3*S*,4*R*,4a*R*,6*S*,7*S*,8*R*,8a*S*,8b*R*,9*S*,9a*S*)-dodecahydro-

4,6,7,8a,8b,9a-hexahydroxy-3,6a,9-trimethyl-7-(1-methylethyl)-6,9-methanobenzo[1,2]pentaleno[1,6-*bc*]furan-8-yl ester (ryanodine) and 1-[6-[[(17β)-3-Methoxyestra-1,3,5(10)-trien-17-yl]amino]hexyl]-1*H*-pyrrole-2,5-dione (U73122) were dissolved in intracellular solution and applied *via* the patch recording. DHPG, dissolved in external solution, was applied through a pipette positioned near the PN dendrite using 20 ms pulses of pressure provided by a pressure ejector PDES-2DX (npi, Tamm, Germany). AmmTx, dissolved in external solution, was applied through a pipette positioned near the PN dendrite by continuous gentle pressure application. CPCCOEt, Heparin sodium salt, ryanodine, U73122, NNC550396 and DHPG were purchased from Tocris (Bristol, UK). IEM1460 was purchased from Hello Bio (Bristol, UK). AmmTx was purchased from Smartox Biotechnology (Saint Egrève, France).

OPTICAL RECORDING

OG5N (Invitrogen, Carlsbad, CA) was excited at 470 nm with an OptoLED (Cairn Research, Faversham, UK) as previously described (Jaafari et al., 2014; Jaafari and Canepari, 2016; Ait Ouares et al., 2016; Ait Ouares et al., 2019). Fura-2FF (Santa Cruz, Dallas, TX) and Fura-2 (Invitrogen) were excited at 385 nm using the OptoLED. V_m and Ca^{2+} optical measurements were achieved sequentially (Canepari and Ogden, 2008) by alternating excitation of Fura-2FF excitation and the excitation of the voltage sensitive dye JPW1114 (Invitrogen) at 528 nm using a LDI laser (89 North, Williston, VT). OG5N Ca^{2+} fluorescence was recorded at 530 ± 21 nm. Fura-2FF and Fura2 Ca^{2+} fluorescence was recorded at 510 ± 41 nm. JPW1114 V_m fluorescence was recorded at >610 nm. Image sequences were recorded using a NeuroCCD-SMQ camera (RedShirtimaging, Decatur, GA). Images were de-magnified by ~0.2X to visualise an area of ~150 µm diameter and acquired at 5 kHz or at 20 kHz with a resolution of 26 X 26 pixels or 26 X 4 pixels respectively. In all experiments, four trials with a 20 s interval between two consecutive trials, were obtained to assess the consistency of the signals and averaged to improve the signal-to-noise ratio. The number of averaged trials was nine in 20 kHz recordings. However, in all figures, the somatic V_m recording used in the illustrations was from a single trial, corresponding to the first trial of the series. Fluorescence was corrected for bleaching using a filtered trial without signal. Ca^{2+} fluorescence transients were expressed as fractional changes of fluorescence ($\Delta F/F_0$), using the average of the first four images of the sequence to calculate F_0. In the colour-coded images, all pixels with intensity value below twice the minimum are set to 1, to exclude pixels with large photon noise threshold, and only those pixels having signal peak >5 % are illustrated, in order to appreciate the signal localisation. V_m fluorescence transients were calibrated in mV using prolonged hyperpolarising steps as described in a previous article (Ait Ouares et al., 2019).

MODEL AND COMPUTER SIMULATIONS OF CALCIUM BINDING TO THE INDICATORS

A simplified version of the model described in Ait Ouares et al., (2016) was used to estimate the Ca^{2+} fluorescence signals in the presence of 2 mM OG5N and 400 µM Fura2. The model consists on a set of 9 equations:

$$\frac{d\left[Ca^{2+}\right]}{dt} = \xi_{Ca} - \sum_{j=1}^{4} \left(K_{ON}^{B_j} \cdot [B_j] \cdot \left[Ca^{2+}\right] - K_{OFF}^{B_j} \cdot \left[B_j Ca^{2+}\right]\right.$$

$$\frac{d\left[B_jCa^{2+}\right]}{dt} = K_{ON}^{B_j}\cdot\left[Ca^{2+}\right]\cdot[B_j]-K_{OFF}^{B_j}\cdot\left[B_jCa^{2+}\right]$$

$$\frac{d[B_j]}{dt} = -\frac{d\left[B_jCa^{2+}\right]}{dt}$$

This model comprises 4 buffers, with association and dissociation constants K_{ON}^{Bj} and K_{OFF}^{Bj} respectively. Buffers 1 and 2 are the indicators OG5N and Fura2 respectively, having K_{ON}^{Fura2} = 570 μM^{-1} s^{-1} (Canepari and Mammano, 1999) and K_D (K_{OFF}/K_{ON}) equal to 35 µM and 0.2 µM respectively. Buffers 3 and 4 are the two pairs of binding sites of calbindin D-28k having K_{ON} equal to 217.5 μM^{-1} s^{-1} and to 27.5 μM^{-1} s^{-1} and K_{OFF} equal to 35.8 s^{-1} nM and 2.6 s^{-1} respectively, as used in Ait Ouares et al., 2019, to take into account the difference in temperature and the radial diffusion from the published values (Nägerl et al., 2000). Calbindin D-28k dominates Ca^{2+} binding in the millisecond time scale (Schmidt and Eilers, 2009) and has estimated concentration of 120 µM (Kosaka et al., 1993). The Ca^{2+} influx associated with the CF was approximated by a Gaussian function of 15 or 20 µM/ms and 1.5 ms time constant, consistent with the detailed model described in Ait Ouares et al. (2019). We simulated 200 ms of recording using the function "ode45" in Matlab. In these 200 ms, the Gaussian function approximating the CF associated Ca^{2+} influx was delayed by 180 ms from the beginning of the simulation and, in the simulations corresponding to the paired scenarios, it was preceded by a slow Ca^{2+} influx approximated by another Gaussian function of 4 µM/ms and 45 ms time constant to estimate the effect of saturating the high affinity buffers. The OG5N $\Delta F/F_0$ signal was extrapolated from the Ca^{2+} bound to the indicator using the dynamic range of 15 measured in Ait Ouares et al (2016). The Fura2 -$\Delta F/F_0$ signal was extrapolated from the Ca^{2+} bound to the indicator using the dynamic range of 0.9 as used in Ait Ouares et al (2019).

EXPERIMENTAL DESIGN AND STATISTICAL ANALYSIS

Data were processed and analysed using MATLAB. Changes produced by the pairing protocol with respect to the CF stimulation alone, or by the pharmacological action of an agent, were assessed by performing the paired Student's t-test on the signal parameter under the two different conditions. A change in the signal was considered significant when $p < 0.01$. In all figures, a significant change was indicated with "*". In the specific case of data reported in Fig. 1, the conclusion that the effect of adding CPCCOEt is different when the CF stimulation is delayed by 60 ms from the first PF stimulus, with respect to the cases of 100 ms and 150 ms delays, is supported by a paired t-test performed on the $\Delta F/F_0$ ratios at two different delays that gave a value of $p < 0.01$.

For the quantitative interpretation of the results of combined Ca^{2+} imaging with the low-affinity indicator OG5N and with the high affinity indicator Fura2, we calculated the variable "*S*" defined as:

$$S = \begin{cases} \dfrac{paired\ \Delta F/F_0\ (hyp)}{unpaired\ \Delta F/F_0\ (hyp)}\ if\ \text{the initial}\ V_m is\ at\ hyp\ state \\ \dfrac{paired\ \Delta F/F_0\ (rest)}{unpaired\ \Delta F/F_0\ (rest)}\ if\ \text{the initial}\ V_m is\ at\ rest\ state \end{cases}$$

It must be noticed that *S* is principally used to analyse the supralinear Ca^{2+} signal at the *hyp* and at the *rest* states and therefore both the numerator the denominator are different according to the different initial V_m. If a supralinear Ca^{2+} signal occurs when a CF-EPSP is evoked under two different conditions, for

instance unpaired and paired, then *S*(OG5N) is obviously positive since a larger free Ca^{2+} concentration implies a larger fraction of Ca^{2+} bound to the low-affinity indicator OG5N. The parameter *S*(Fura2) can unambiguously discriminate whether a supralinear Ca^{2+} signal is or is not exclusively due to the saturation of Fura2, and whether it is or it is not exclusively due to a larger Ca^{2+} influx through the plasma membrane.

1. *Case of supralinear Ca^{2+} signal exclusively due to the saturation of Fura2*. In the presence of Fura2, the larger fraction under paired conditions can be in principle exclusively due to the saturation of the high-affinity indicator by the Ca^{2+} associated with the PF stimulation. Thus, if less free Fura2 is available to buffer the Ca^{2+} entering the cell during the CF-EPSP, more Ca^{2+} will bind to OG5N and less Ca^{2+} will bind to Fura2 under paired conditions, implying that *S*(Fura2) will be smaller than 1. Thus, if *S*(Fura2) is larger than 1, it unambiguously proves that the supralinear Ca^{2+} signals is not exclusively due to the saturation of Fura2, i.e. that at least a fraction Ca^{2+} bound to the low-affinity indicator OG5N originates from Ca^{2+} influx through the plasma membrane.
2. *Case of supralinear Ca^{2+} signal exclusively due to Ca^{2+} influx through the plasma membrane*. If the concentration of Fura2 bound to Ca^{2+} associated with the PF stimulation is negligible with respect to the free Fura2 concentration at the time of the CF-EPSP, then the Ca^{2+} transient entering the cell will linearly bind to OG5N and to Fura2, implying that *S* will have the same value for the two indicators. Thus, if the ratio *S*(Fura2)/*S*(OG5N) = 1, this means that Fura2 is not saturated. Alternatively, if *S*(Fura2)/*S*(OG5N) < 1, this means that at least a fraction Ca^{2+} bound to the low-affinity indicator OG5N originates from the saturation of Fura2.

In the specific case in which the unpaired Ca^{2+} signal is the same, i.e. when the initial V_m is at the *hyp* state and the delay of the CF stimulation is either 60 ms or 110 from the first PF stimulus, the ratio *S*(Fura2)/*S*(OG5N) provides a comparative estimate of the Fura2 saturation. Indeed, regardless of the contribution of the Ca^{2+} influx that is different at the two different delays, the more Fura2 is saturated the smaller *S*(Fura2) will be and, conversely, the larger *S*(OG5N) will be. Thus, the smaller *S*(Fura2)/*S*(OG5N) is, the larger the contribution of Fura2 saturation will be.

Results

Distinct dendritic supralinear Ca^{2+} transients associated with paired PF-CF stimulation

Several studies have shown that, at sites of activated PF synapses, the Ca^{2+} transient associated with a CF-EPSP is significantly larger when it occurs after PF activation (Wang et al., 2000; Brenowitz and Regehr, 2005; Safo and Regehr, 2005; Canepari and Vogt, 2008). To initially analyse these supralinear Ca^{2+} signals, we used a protocol of stimulation for the PF input consisting of 5 stimuli delivered at 100 Hz with an electrode positioned near a PN dendritic site (Fig. 1A), with the initial V_m hold between -75 mV and -85 mV, below the average V_m recorded in the soma when no current is injected (V_{rest}), which was always between -65 mV and -50 mV. The intensity of stimulation was set to attain a first EPSP in the range of 1-4 mV of somatic amplitude and the protocol occasionally caused somatic action potentials during the last EPSPs. In cells filled with 2 mM of the low-affinity Ca^{2+} indicator OG5N (K_D = 35 µM, Canepari and Ogden,

2006), this protocol systematically produced a fast fractional change of fluorescence ($\Delta F/F_0$) signal, raising at each individual PF-EPSP, followed by a slow $\Delta F/F_0$ signal peaking at 100-150 ms after the first PF stimulus. As illustrated by the colour code pictures in Fig. 1A, both signals were localised within the same area of a few microns adjacent to the PF stimulating electrode since the sharp depolarisation associated with PF-EPSPs is also localised (Canepari and Vogt, 2008). At submicron spatial scale, however, the two signals are probably not co-localising, since the fast signal is mediated by VGCCs activated by the PF depolarisation (Canepari and Vogt, 2008), whereas the slow signal is mediated by a non selective cation conductance (Canepari et al., 2004) which is believed to be formed by TRPC3 channels (Hartmann et al., 2008).

The time course of the Ca^{2+} transient in the 2X2 pixels (~11X11 μm^2) region (*R1*) adjacent to the PF stimulating electrode is reported together with $\Delta F/F_0$ from a control region (*R2*) of the same size with no Ca^{2+} signal to show the high signal-to-noise ratio of these measurements permitting a precise quantitative analysis of Ca^{2+} signals. We investigated the Ca^{2+} signal associated with a CF-EPSP unpaired or paired with the PF-EPSPs at delays of 60 ms, 100 ms or 150 ms from the first PF stimulus (Fig. 1B). In all three cases, the Ca^{2+} transient associated with the paired CF-EPSP was larger than that associated with the unpaired CF-EPSP and these phenomena were restricted to the area where the two Ca^{2+} transients associated with the PF-EPSPs were observed, as illustrated by the colour code frames in Fig. 1B. Addition of the mGluR1 inhibitor CPCCOEt (20 µM) reduced the slow $\Delta F/F_0$ signal associated with PF stimulation (Fig. 1C) and the supralinear Ca^{2+} signals associated with the CF-EPSP delayed by 100 ms and 150 ms from the first PF stimulus, but not that associated with the CF-EPSP delayed by 60 ms from the first PF stimulus. In N = 6 cells, we quantified the supralinear Ca^{2+} signal by calculating the ratio between the amplitude of the $\Delta F/F_0$ signal associated with the paired CF-EPSP and the amplitude of the $\Delta F/F_0$ signal associated with the unpaired CF-EPSP ($\Delta F/F_0$ ratio, Fig. 1D). The $\Delta F/F_0$ ratio significantly ($p < 0.01$, paired t-test) decreased from 3.40 ± 0.73 to 1.93 ± 0.42 and from 3.38 ± 0.69 to 2.02 ± 0.27 in the cases of 100 ms and 150 ms delay of the CF stimulation respectively. In contrast, it did not significantly ($p > 0.1$, paired t-test) change (from 2.23 ± 0.47 to 2.19 ± 0.60) in the case of 60 ms delay of the CF stimulation. We concluded that supralinear Ca^{2+} signals associated with CF-EPSPs delayed by 100 ms and 150 ms were mGluR1-dependent, whereas the supralinear Ca^{2+} signal associated with the CF-EPSP delayed by 60 ms was mGluR1-independent.

The CF-associated Ca^{2+} transient at initial hyperpolarised V_m (*hyp*, ~-80 mV) is mainly mediated by Ca^{2+} influx *via* T-type VGCCs (Ait Ouares et al., 2019). Thus, we further investigated the supralinear Ca^{2+} signal at V_{rest} (*rest*, ~-60 mV), i.e. when T-type VGCCs are mostly inactivated and the CF-associated Ca^{2+} transient is largely mediated by Ca^{2+} influx *via* P/Q-type VGCCs that can be activated because also most of A-type K^+ channels are inactivated. Again, we used the protocol consisting of 5 PF stimuli at 100 Hz with an electrode positioned near a PN dendritic site (Fig. 2A), followed by a CF-EPSP delayed by 110 ms from the first PF stimulus. In this experiment, however, recordings were performed both at *hyp* and *rest* initial V_m (Fig. 2B). In both cases, the Ca^{2+} transient associated with the paired CF-EPSP was larger than that associated with the unpaired CF-EPSP, and both supralinear Ca^{2+} signals were co-localised with the PF active area (see the colour code frames in Fig. 2B). Addition of CPCCOEt reduced both supralinear

Ca^{2+} signals associated with the CF-EPSP (Fig. 2C). In N = 6 cells, the $\Delta F/F_0$ ratio significantly ($p < 0.01$, paired t-test) decreased from 3.02 ± 0.61 to 1.88 ± 0.50 and from 2.19 ± 0.38 to 1.46 ± 0.30 in the cases of *hyp* and *rest* initial V_m respectively (Fig. 2D). We concluded that supralinear Ca^{2+} signals associated with CF-EPSPs, delayed by 110 ms from the first PF stimulus, were mGluR1-dependent both at *hyp* and at *rest* initial V_m, i.e. independently on whether the CF-associated Ca^{2+} transient is mediated by T-type or P/Q-type VGCCs.

Kinetics of dendritic supralinear Ca^{2+} signals

The three forms of supralinear Ca^{2+} signals presented in the previous paragraph are time-correlated with the CF-associated Ca^{2+} transients which are mediated by T-type and P/Q-type VGCCs (Ait Ouares et al., 2019). They can be in principle due to the modulation of these Ca^{2+} sources, to the activation of other Ca^{2+} sources, or to both phenomena. If it is only the original Ca^{2+} source to be larger, then the kinetics of the rising phase of the Ca^{2+} transient is expected to be the same for the paired and unpaired CF signal. Thus, useful information can be obtained by analysing the kinetics of the rising phase of the Ca^{2+} transients in paired protocols with respect to the Ca^{2+} transients associated with unpaired CF-EPSPs, to reveal any possible subsequent component of the Ca^{2+} transients. To this aim, we performed Ca^{2+} recordings associated with the same stimulation protocols described in the previous paragraph, but in this case at 20 kHz to accurately analyse the kinetics of Ca^{2+} transients (Fig. 3A). We then analysed the rising phase of the different Ca^{2+} transients exploiting the short relaxation time of OG5N (Jaafari et al., 2015; Jaafari and Canepari, 2016; Ait Ouares et al., 2016). To quantitatively analyse the fast kinetics of Ca^{2+} transients, we averaged 9 recordings for each stimulating protocol (instead of 4). As shown in Fig. 3A, the individual somatic V_m signals and the associated Ca^{2+} transients were perfectly aligned indicating no jitter in the timing of the CF stimulation. We then normalised the signals to the peak and applied a Savitzky-Golay smoothing filter (Fig. 3B) with 20 points time window, that reduces the noise with minimal distortion of the kinetics of the fluorescence transient (Savitzky and Golay, 1964), as previously demonstrated (Jaafari et al., 2015). Finally, we calculated the time derivative (Jaafari et al., 2014) as shown in Fig. 3C. The time to peak of the time derivative, from the CF stimulus, is an indirect kinetics measurement of the Ca^{2+} source and it is typically longer for T-type VGCCs that principally mediate Ca^{2+} influx at *hyp* states, with respect to P/Q-type VGCCs that principally mediate Ca^{2+} influx at *rest* states (Ait Ouares et al., 2019). Thus, in the example of Fig. 3C, the time difference between the two peaks (Δt_{peak}) at the *hyp* and the *rest* state, in the case of unpaired CF-EPSPs, was 3 samples (150 µs). We then measured the times to peak in the cases of CF-EPSPs in pairing protocol and compared those with the cases of unpaired CF-EPSPs. In the example of Fig. 3C, the time to peak of the paired CF signal at the *hyp* state was the same of that of unpaired CF signal at the *hyp* state ($\Delta t_{peak} = 0$). In contrast, the times to peak of the paired CF signal at the *rest* state or with the CF stimulation delayed by 60 ms from the first PF stimulus were the same of that of unpaired CF signal at the *rest* state. We performed this analysis in N = 8 cells and calculated both Δt_{peak} from the CF signal at *hyp* (Fig. 3D, top bar diagram) and at *rest* states (Fig. 3D, bottom bar diagram). The time to peak of the paired CF signal at *hyp* states was the same of the unpaired CF signal at *hyp* states and the time to peak of the paired CF signal at *rest* states was the same of the unpaired CF signal at *rest*

states. In contrast, the time to peak of the CF signals (paired and unpaired) at *hyp* states was significantly ($p<0.01$ paired t-test) longer (by 2.75 ± 0.71 samples) from the time to peak of the CF signals (paired and unpaired) at *rest* states. Finally, the time to peak of the CF signals at *hyp* states was significantly ($p<0.01$ paired t-test) longer (by 2.38 ± 0.75 samples) than the time to peak of the paired CF signals with the CF stimulation delayed by 60 ms from the first PF-stimulus. We therefore concluded that the fast kinetics of Ca^{2+} transients associated with the CF-EPSP is identical in paired and unpaired condition, both at *hyp* and *rest* states, when the CF stimulation is delayed by 110 ms from the first PF stimulus. This conclusion suggests that the principal Ca^{2+} source of the supralinear Ca^{2+} signal with the CF stimulation delayed by 110 ms from the first PF stimulus at *hyp* states is the T-type VGCC. In contrast, the principal Ca^{2+} source of the supralinear Ca^{2+} signals with the CF stimulation delayed by 110 ms from the first PF stimulus at *rest* states, or with the CF stimulation delayed by 60 ms from the first PF stimulus, is likely the P/Q-type VGCC.

Yet, several studies have linked PF-triggered activation of mGluR1s to Ca^{2+} release from internal stores, in particular via InsP3 receptors (Finch and Augustine, 2018; Takechi et al., 1998). To directly test whether Ca^{2+} release from internal stores play a role in these supralinear Ca^{2+} signals, we performed experiments with the internal solution containing either 1 mg/mL of heparin (Fig. 4A), to inhibit Ca^{2+} store release *via* InsP3 receptors (Kim et al., 2008), or with the internal solution containing 100 µM ryanodine (Fig. 4B), to inhibit Ca^{2+} store release *via* ryanodine receptors (Kano et al., 1995). In groups of 6 cells tested with each pharmacological agent, mGluR1-dependent supralinear Ca^{2+} transients were consistent with those measured in control internal solution (Fig. 4C). The same result was obtained in a group of 6 cells, tested at *hyp* states only, injected with 10 µM of the phospholipase-C inhibitor U73122 (data not shown), that was proven to prevent mGluR1-mediated Ca^{2+} release from stores in PN dendrites (Canepari and Ogden, 2006). Taken together, these results rule out any significant contribution of Ca^{2+} release from stores either *via* InsP3 or ryanodine receptors.

Dendritic V_m associated with mGluR1-dependent supralinear Ca^{2+} signals

Since Ca^{2+} release from internal stores does not contribute to the supralinear Ca^{2+} signals reported above, the origin of these phenomena can be an increase in the Ca^{2+} influx through the plasma membrane during the CF-EPSP, an increase in free Ca^{2+} concentration (and therefore in the Ca^{2+} bound to the OG5N) due to a transient saturation of endogenous Ca^{2+} buffers or a combination of both phenomena. If the supralinear Ca^{2+} signal includes an increase of Ca^{2+} influx through the plasma membrane, the additional charge influx is expected to increase the electrical current and therefore the dendritic V_m transient associated with the CF-EPSP. We initially measured dendritic V_m associated with a paired CF-EPSP delayed by 60 ms from the first PF stimulus using V_m imaging from a region adjacent to the PF stimulation electrode. V_m fluorescence transients were calibrated on an absolute scale (in mV) using prolonged hyperpolarising pulses as previously described (Canepari and Vogt, 2008; Ait Ouares et al., 2019), to quantify the depolarisation associated with the CF-EPSP under different conditions. In the experiment reported in Fig. 5A, the initial V_m before the CF-EPSP shifted from -80 mV to -62 mV when the PF-EPSP train was applied (Fig. 5B). Consistently with the fact at that this initial V_m A-type K^+ channels

are partially inactivated, and activation of P/Q-type VGCCs is boosted (Ait Ouares et al., 2019), the peak V_m shifted from -21 mV to -3 mV. Significant shifts in the initial and peak V_m were observed in N = 8 cells in which this experiment was performed (Fig. 5C), confirming that the mGluR1-independent supralinear Ca^{2+} signal, occurring when the CF-EPSP is at the end of the PF-EPSPs train, is associated with a shift from T-type VGCCs to P/Q-type VGCCs as suggested by the results reported in Fig. 3.

After this first set of V_m experiments, we performed combined V_m and Ca^{2+} imaging recordings with a similar approach recently utilised to characterise the dendritic V_m transient associated with the unpaired CF-EPSP (Ait Ouares et al., 2019), to measure dendritic V_m associated with mGluR1-dependent supralinear Ca^{2+} signals. The cell shown in Fig. 6A was filled with the voltage-sentive dye (VSD) JPW1114 and with 1 mM of the low-affinity Ca^{2+} indicator Fura-2FF (K_D = 6 µM, Hyrc et al., 2000), used to localise the area of supralinear Ca^{2+} signals both at *hyp* and *rest* initial V_m (Fig. 6A). Consistently with the observation that PF-ESPSs locally activate VGCCs at *hyp* initial V_m, the depolarisation associated with the PF train was above -30 mV in the region (*R1*) adjacent to the stimulating electrode, while the depolarisation was comparable with that in the soma in a different region (*R2*), as shown in Fig. 6B. To excite VSD fluorescence over 160 ms without causing photodamage, we used only 20% of the laser intensity applied for previous CF-associated V_m measurements (Ait Ouares et al., 2019). Using this weaker illumination, the standard deviation of the photon noise was equivalent to ~2.5 mV after calibration and the peak-to-peak noise was equivalent to ~10 mV in *R1* (Fig. 6B). Therefore, to allow discrimination of V_m changes of less than 3 mV, we applied the following filtering procedures (Fig. 6C). For the unpaired CF recordings, the initial V_m was set to the averaged V_m signal before CF stimulation. For the paired CF recordings, the initial V_m was accurately estimated by applying a 64-points median filter to the original fluorescence signal after the end of the PF stimulation. Finally, for all recordings, a 4-points median filter was applied to the 20 ms fluorescence signal following CF stimulation. Fig. 6D shows a small but detectable additional depolarisation associated with the paired CF-EPSP both at *hyp* and *rest* initial V_m. In N = 7 cells, in which we successfully performed combined V_m and Ca^{2+} with filtered signals above the photon noise to discriminate V_m changes < 3 mV, the additional depolarisation, calculated as the difference between the paired and unpaired CF-associated V_m transients was always detectable in the case of *hyp* initial V_m and corresponded to a significant increase of 5.0 ± 1.6 mV ($p < 0.01$, paired t-test). In the case of *rest* initial V_m, a detectable increase (>3 mV) was observed only in 4/7 cells. The mean ± SD of the V_m was 2.5 ± 2.5 mV (N = 7 cells). We concluded that small additional V_m transients are always associated with mGluR1-dependent supralinear Ca^{2+} signals at *hyp* initial V_m, a result consistent with the hypothesis that at least part of the supralinear Ca^{2+} signal under this condition is due to Ca^{2+} influx through the plasma membrane. In the case of *rest* initial V_m, additional V_m transients were occasionally observed, suggesting a smaller and possibly highly variable contribution of Ca^{2+} influx through the plasma membrane.

Contribution of the saturation of the endogenous buffer to the supralinear Ca^{2+} signals

In a previous study we have shown that trains of PF stimuli at 100 Hz produce a local progressive saturation of endogenous Ca^{2+} buffers that boosts a Ca^{2+} fluorescent transient associated with a CF-EPSP

occurring at the end of the PF train (Canepari and Vogt, 2008). Since mGluR1 activation induces a slow Ca^{2+} influx, saturation of the endogenous Ca^{2+} buffer may occur on a longer time scale and contribute to the mGluR1-dependent supralinear Ca^{2+} signals. To test whether this phenomenon occurs, experiments can be performed with the inclusion the high-affinity UV-excitable indicator Fura-2 (Fura2, K_D ~200 nM). We initially tested different Fura2 concentrations (100 µM, 200 µM and 400 µM) and we finally chose the concentration of 400 µM since under this condition the Fura2 signal was not saturated by a CF Ca^{2+} transient and the OG5N was still large enough to be accurately analysed. To examine quantitatively how this type of measurement can provide an answer to the question on whether and at which extent the saturation of the endogenous buffer contributes to the supralinear Ca^{2+} signals, we run computer simulations using the simple but realistic biochemical model described in the Materials and Methods. Specifically, we analysed a scenario where the same Ca^{2+} influx associated with a CF-EPSP occurs unpaired or paired with a previous slow Ca^{2+} influx, and another scenario in which the paired Ca^{2+} influx is 25% larger with respect to the unpaired Ca^{2+} influx (Fig. 7A). When the simulation is run without Fura2, the putative OG5N $\Delta F/F_0$ exhibits supralinear Ca^{2+} signals under paired conditions in both scenarios (Fig. 7B). When the simulation is instead run with Fura2, while supralinear Ca^{2+} signals under paired conditions are still present in the putative OG5N $\Delta F/F_0$, the putative Fura2 $-\Delta F/F_0$ behaves differently in the two scenarios: it exhibits a small supralinear Ca^{2+} signal in the case of potentiated Ca^{2+} influx, but the paired Ca^{2+} signal is smaller than the unpaired Ca^{2+} signal when Ca^{2+} influx is the same (Fig. 7C). To analyse quantitatively this result, we introduce the variable "*S*" defined as the ratio of the paired $\Delta F/F_0$ peak against the unpaired $\Delta F/F_0$ peak. The conclusive information that can be obtained, by the analysis of the variable *S*, is explained in detail in the *Experimental design and statistical analysis* section of the Materials and Methods. Briefly, when the supralinear Ca^{2+} signal is exclusively due to buffer saturation, then the value of *S* for Fura2 (S_{Fura2}) must be less than one (S_{Fura2} = 0.95 in the case of the simulation of Fig. 7C). In contrast, a value of S_{Fura2} larger than 1 indicates that larger Ca^{2+} influx contributes to the supralinear Ca^{2+} signal (S_{Fura2} = 1.22 in the case of the simulation of Fig. 7C). Since a supralinear Ca^{2+} signal exclusively due to larger Ca^{2+} influx (i.e. no buffer saturation) leads to an increase in the absolute $\Delta F/F_0$ signal which is the same for the two indicators, the ratio of *S* for the two indicators (S_{Fura2}/S_{OG5N}) must be 1 in this case. It follows that a lower value of this ratio indicates that buffer saturation contributes to the supralinear Ca^{2+} signal (S_{Fura2}/S_{OG5N} = 0.54 in the case of the simulation of Fig. 7C). Thus S_{Fura2}/S_{OG5N} also represents a quantitative estimate of the extent of buffer saturation in the two cases. With the premise that the analysis of the saturation of Fura2 provides an estimate for the saturation of the endogenous buffer occurring physiologically, we run experiments by adding 400 µM Fura2 in the patch electrode. In the cell of Fig. 8A, we applied the same stimulation protocols of Fig. 3 and measured separately the absolute fluorescent transients from the two indicators (OG5N $\Delta F/F_0$ and Fura2 $-\Delta F/F_0$). Under this condition, supralinear OG5N Ca^{2+} signals were observed (Fig. 8B), indicating that these signals are not prevented by the presence of Fura2 at this moderate concentration. In contrast, whereas a supralinear Fura2 Ca^{2+} signal associated with the paired CF-EPSP delayed by 110 ms at the *hyp* state was observed, the Fura2 Ca^{2+} signal associated with the paired CF-EPSP delayed by 60 ms was smaller than the Ca^{2+} signal associated with the unpaired CF-EPSP (Fig. 8B). We then calculated the variable *S* for the ratios of the

$\Delta F/F_0$ peaks in each protocol against the $\Delta F/F_0$ peak associated with the unpaired CF stimulation (Fig. 8C). In N = 8 cells tested, S_{Fura2} was significantly positive for the mGluR1-dependent supralinear Ca^{2+} signal at *hyp* states ($p<0.01$ paired t-test, $S_{Fura2} = 2.38 \pm 0.05$), confirming that larger Ca^{2+} influx through the plasma membrane contributes in this case (Fig. 8C). However, S_{Fura2} was significantly smaller than S_{OG5N} ($p<0.01$, paired t-test, $S_{Fura2}/S_{OG5N} = 0.58 \pm 0.09$) indicating that also buffer saturation contributes to this supralinear Ca^{2+} signal. Finally, S_{Fura2}/S_{OG5N} for the mGluR1 independent supralinear Ca^{2+} signal (0.31 ± 0.13) was significantly smaller than S_{Fura2}/S_{OG5N} for the mGluR1-dependent supralinear Ca^{2+} signal ($p<0.01$, paired t-test), indicating that in this case buffer saturation provides a larger contribution. The Ca^{2+} increase through P/Q-type VGCCs produced by switching from *hyp* states to *rest* states is essentially due to larger Ca^{2+} influx ($S_{Fura2}/S_{OG5N} = 0.80 \pm 0.23$). Thus, as expected, the further mGluR1-dependent Ca^{2+} increase includes a significant contribution of buffer saturation ($S_{Fura2}/S_{OG5N} = 0.54 \pm 0.19$, calculated using the unpaired CF signal at *rest* states). This analysis, however, does not allow estimating a possible contribution of larger Ca^{2+} influx in the case of mGluR1-dependent supralinear Ca^{2+} signal at *rest* states.

Origin of the mGluR1-dependent supralinear Ca^{2+} signals at initial hyperpolarised V_m

The results presented above demonstrate that mGluR-dependent supralinear Ca^{2+} signals at the *hyp* state are due to a combination of Ca^{2+} influx increase through the plasma membrane and to a transient saturation of the endogenous Ca^{2+} buffer. The rising phase of the paired CF Ca^{2+} signal has the same kinetics of the Ca^{2+} signal associated with the unpaired CF input (Fig. 3) which is principally mediated by T-type VGCCs (Ait Ouares et al., 2019). It has been reported that mGluR1 activation potentiate Cav3.1 T-type VGCCs in PNs (Hildebrand et al., 2009). Hence, we finally assessed directly whether the Ca^{2+} influx component of the mGluR1-dependent supralinear Ca^{2+} signal at *hyp* states is through these channels. In the cell reported in Fig. 9A, we recorded the Ca^{2+} transient associated with a CF-EPSP unpaired or paired with PF stimulation, at *hyp* or *rest* initial V_m in control conditions with a delay of 110 ms from the first PF stimulus and the CF stimulation. Addition of 30 µM of the Cav3.1 blocker NNC550396 (NNC) inhibited spontaneous firing at *rest* initial V_m and strongly reduced Ca^{2+} transients associated both with PF-EPSPs and the CF-EPSP at *hyp* initial V_m (Fig. 9A). In contrast, Ca^{2+} transients associated both with PF-EPSPs and the CF-EPSP at *rest* initial V_m were only slightly affected by NNC addition, confirming that dendritic T-type VGCCs are mostly inactivated at this state (Fig. 9A). As shown in Fig. 9B, the supralinear Ca^{2+} transient at *hyp* initial V_m was also strongly inhibited by addition of NNC. In N = 6 cells tested with this experimental protocol, the ratios between the CF Ca^{2+} signals in the presence of NNC and in control condition at initial hyperpolarised V_m were 0.44 ± 0.18 and 0.32 ± 0.13 for the CF unpaired or paired with PF stimulation respectively (Fig. 9C). In both cases, the Ca^{2+} signal associated with the paired CF-EPSP was significantly smaller ($p< 0.01$, paired t-test). In contrast, the ratios between the CF Ca^{2+} signals in the presence of NNC and in control condition at *rest* initial V_m were 0.93 ± 0.13 and 0.91 ± 0.10 for the CF unpaired or paired with PF stimulation respectively, indicating that in this state T-type VGCCs contribute marginally to Ca^{2+} signals (Fig. 9C). The results reported in Fig. 9 unambiguously confirm that the Ca^{2+} influx component responsible for mGluR1-dependent supralinear Ca^{2+} signals at *hyp* state is mediated by T-type Ca^{2+} channels.

As shown in the example of Fig. 9A, addition of NNC reduced the fast Ca^{2+} transient associated with the PF-EPSP train while it did not affect the slow Ca^{2+} transient mediated by mGluR1s. Furthermore, although both unpaired and paired Ca^{2+} transients were inhibited by NNC, the paired Ca^{2+} transient was still larger (Fig. 9A), suggesting that local amplification of the residual component by buffer saturation is still present when T-type VGCCs are blocked. Thus, endogenous buffer is likely saturated by the slow mGluR1-mediated Ca^{2+} influx. To test this hypothesis, we measured mGluR1-dependent supralinear Ca^{2+} signals at *hyp* states while blocking the slow mGluR1-mediated Ca^{2+} transient with the channel blocker IEM1460 that does not affect the mGluR1-dependent boosting of T-type VGCCs (Hildebrand et al., 2009). In the example of Fig. 10A, addition of 250 µM of IEM1460 produced a use dependent block of the slow mGluR1-dependent Ca^{2+} transient over a period of 20 minutes in which stimulation protocols were repeated every 5 minutes. While a change in the somatic V_m recordings was observed after IEM1460 application, the fast PF-mediated Ca^{2+} transients did not change indicating that VGCCs were not directly affected by the blocker. Whereas the Ca^{2+} transient associated with the unpaired CF-EPSP was also not affected, the Ca^{2+} transient associated with the paired CF-EPSP was progressively reduced consistently with the slow mGluR1-mediated Ca^{2+} transient that was extrapolated using a simple fitting of the decay phase of the fast PF-mediated Ca^{2+} transient (Fig. 10B). We performed this experiment in N = 6 cells, obtaining a significant reduction of the slow mGluR1-mediated Ca^{2+} transient ($p<0.01$, paired t-test), 20 minutes after IEM1460 application, corresponding to a $\Delta F/F_0$ ratio of 0.49 ± 0.16 (Fig. 10C). Consistently with this result, the supralinear Ca^{2+} signal, quantified again as the ratio between the paired and the unpaired $\Delta F/F_0$ peaks, significantly ($p < 0.01$, paired t-test) decreased from 3.37 ± 0.83 to 1.86 ± 0.56 (Fig. 10D). We concluded that the mGluR1-dependent supralinear Ca^{2+} signal at *hyp* states are caused by boosting of T-type VGCCs amplified by endogenous buffer saturation produced by the slow mGluR1-dependent PF-mediated Ca^{2+} influx.

Origin of the mGluR1-dependent supralinear Ca^{2+} signals at V_{rest}

The experiments reported in Fig. 8 and in Fig. 10 suggest that the mGluR1-dependent supralinear Ca^{2+} signal also at *rest* state is largely due to saturation of the endogenous buffer, but the results reported in Fig. 9 further suggest that an increase in Ca^{2+} influx may contribute in a variable manner. It has been reported that mGluR1 activation shifts the inactivation curve of A-type K^+ channels boosting the opening of P/Q VGCCs at initial V_m > -65 mV in PNs (Otsu et al., 2014). Thus, consistently with the results of the kinetics analysis reported in Fig. 3, an increase in Ca^{2+} influx *via* P/Q-type VGCCs may contribute to this supralinear Ca^{2+} signal. In contrast to the direct local regulation of T-type VGCCs by mGluR1s (Hildebrand et al., 2009), occurring at *hyp* states, the indirect regulation of P/Q-type VGCCs is produced by a V_m modulation and therefore it is not co-localised with mGluR1s. By analysing cells in which V_{rest} was <-60 mV, i.e. where A-type K^+ channels are not yet fully inactivated, we observed some occasional small supralinear Ca^{2+} signals at far-away sites from the PF-activated region at *rest* states. An example of this wide supralinear Ca^{2+} signal is reported in Fig. 11A and Fig.10B. While this far supralinear Ca^{2+} signal was smaller than the supralinear Ca^{2+} signal co-localised with the PF-mediated signal (Fig. 11A), the kinetics

was qualitatively similar to that of a "supralinear" Ca^{2+} signal obtained by blocking A-type K^+ channels with the toxin AmmTx3 (Zoukimian et al., 2019; Ait Ouares et al., 2019), as shown in the example of Fig. 11C.

Finally, in many studies, physiological mGluR1 activation has been mimicked by bath application of the agonist (S)-3,5-dihydroxyphenylglycine (DHPG, see for example Canepari et al., 2001; Tempia et al., 2001; Maejima et al., 2005; Otsu et al., 2014). We examined this artificial stimulation protocol, that in principle can also produce Ca^{2+} release from internal stores, by applying 100 µM DHPG, using a pipette positioned near the dendrites, with a short (20 ms) pressure ejection as shown in the example of Fig. 12A. At *hyp* state, DHPG application triggered a slow Ca^{2+} signal, but in contrast to the physiological PF stimulation a corresponding slow V_m depolarisation was observed in the soma (Fig. 12A). Thus, while a substantial supralinear Ca^{2+} signal associated with DHPG pairing was observed, the kinetics of the Ca^{2+} transient indicates a dominance of Ca^{2+} influx via P/Q-type VGCCs (Fig. 12B), consistently with the fact that the initial V_m for the CF-EPSP is ~-60 mV. The size of the supralinear Ca^{2+} signal associated with DHPG application is comparable to those associated with PF stimulation (Fig. 12C). Nevertheless, since all these phenomena are largely due to transient saturation of the endogenous buffer and the spatial and temporal dynamics of Ca^{2+} influx causing this saturation is different in the different protocols, we conclude that experiments using DHPG application cannot realistically mimic the physiological scenarios associated with mGluR1 activation.

In summary, at the *rest* state, regulation of P/Q-type VGCCs by mGluR1 activation may contribute to the supralinear Ca^{2+} signal, but the localisation of this signal, produced by Ca^{2+} influx *via* these channels, is entirely due to the previous Ca^{2+} entry that saturates the endogenous buffer.

Discussion

Determinants of the different dendritic supralinear Ca^{2+} signals in PNs

In this study we identified the biophysical determinants of the dendritic supralinear Ca^{2+} signals, observed when a CF-EPSP is preceded by PF activation, that are believed to trigger PF synaptic plasticity (Hartell, 2002; Jörntell and Hansel, 2006; Vogt and Canepari, 2010). In a recent report, we have demonstrated that isolated CF-EPSPs essentially trigger Ca^{2+} influx *via* T-type VGCCs when the initial V_m < -70 mV and Ca^{2+} influx *via* P/Q-type VGCCs when the initial V_m > -60 mV (Ait Ouares et al., 2019). In both cases these signals are spread throughout the dendritic arborisation at different extent. Here we demonstrate that bursts of PF-EPSPs are capable of locally amplifying these two Ca^{2+} signals at the sites of activated PF synapses, driving the CF "error" signal specifically to these inputs (Safo and Regehr, 2008). The biophysical mechanisms that permit these phenomena of amplification are summarised in Fig. 13. As shown in Fig. 6B, a burst of PF-EPSPs locally depolarises the dendritic area comprising the activated spines. Thus, if a CF-EPSP occurs during this depolarising phase, the Ca^{2+} influx associated with the CF-EPSP will be principally mediated by P/Q-type VGCCs, independently of the initial V_m. The fast Ca^{2+} influx associated with the PF-mediated depolarisation can transiently saturate the endogenous Ca^{2+} buffer and therefore a supralinear free Ca^{2+} signal is produced in the dendritic region where V_m is

depolarised. It must be pointed out that this type of supralinear Ca^{2+} signal depends on the number and arrangement of activated PFs that determine the spatial pattern of depolarisation, but it is not clearly established whether a scenario of "beams" of PF axons activating spines in close proximity occurs *in vivo* (Bower, 2002). During the short PF-mediated depolarisation, mGluR1s do not affect the Ca^{2+} transient associated with the CF-EPSP (Fig. 1D). After the end of the PF train, V_m is repolarised and mGluR1 effects take action. In this time window, if the repolarised V_m is at the *hyp* state (< -70 mV) the Ca^{2+} influx associated with the CF-EPSP will be principally mediated by T-type VGCCs which are potentiated by mGluR1s (Fig. 9). In addition, the slow mGluR1-mediated Ca^{2+} influx is also capable of saturating the endogenous buffer, a mechanism that further amplifies this supralinear free Ca^{2+} signal (Fig. 10). Interestingly, both T channels potentiating and the slow mGluR1-mediated Ca^{2+} influx are triggered by the same mGluR1 pathway (Hildebrand et al., 2009) involving a protein tyrosine phosphatase (Canepari and Ogden, 2003), suggesting that the two factors contributing to this supralinear Ca^{2+} signal co-localise with mGluR1s at submicron scale. Eventually, if the repolarised V_m is > -65 mV, the Ca^{2+} influx associated with a CF-EPSP will be principally mediated by P/Q-type VGCCs. The Ca^{2+} influx via P/Q-type VGCCs can be also boosted by mGluR1s through inhibition of A-type K^+ channels (Otsu et al., 2014), but with two major differences with respect to the T channels boosting discussed above. First, this mechanism is highly variable since at these initial V_m range A-type K^+ channels are already partially inactivated. Second, the potentiated P/Q channels do not co-localise with the site of activated PFs (Fig. 11A and Fig. 11B). Thus, the only mechanism providing co-localisation in this case is saturation of the endogenous buffer produced by the slow Ca^{2+} influx that is independent of the initial V_m.

Role of the initial V_m and implication for synaptic plasticity

The evidence that mGluR1s locally potentiate a specific Ca^{2+} source (the T-type VGCC) and concomitantly amplify the same signal suggests that the occurrence of a *hyp* state episode is important for synaptic plasticity. Yet, *in vivo* electrode recordings have shown that, in PNs, V_{rest} is similar to that observed in brain slices (Kitamura and Häusser, 2011), indicating that the dendritic V_m is normally not at the *hyp* state. Also, spontaneous bursts of dendritic Ca^{2+} spikes are observed by recording Ca^{2+} and V_m signals simultaneously (Roome and Kuhn, 2018), again indicating that depolarising transients occur when the dendrite is relatively depolarised. These observations suggest that the *hyp* state might occur exclusively during rare but crucial episodes in which synaptic plasticity may occur. Episodes of *hyp* state can be due, in principle, to synaptic inhibition coactively occurring during activity patterns associated with cerebellar learning (Suvrathan and Raymond, 2018). Indeed, it was recently demonstrated that optogenetic activation of interneurons in the molecular layer strongly affects PF synaptic plasticity and motor learning, as well as CF-mediated signalling (Rowan et al., 2018; Gaffield et al., 2018). Another possibility is that *hyp* state episodes are intrinsically generated in PNs by a "priming" signal that hyperpolarises the cell, for instance by activating a K^+ conductance. Interestingly, in a recent study, it was proposed that PF synaptic depression may physiologically occur when two CF events occur, the first one concomitant with a PF-EPSP burst and the second one after 100 ms (Bouvier et al., 2018). Notably, the

concomitant activation of PF and CF inputs hyperpolarises the PN, as also visible in the examples with 60 ms delay reported here in Fig. 3A and Fig. 8A.

Role of the mGluR1-activated non-selective cation conductance

An mGluR1-activated non-selective cation conductance, permeable to Ca^{2+}, is the channel that mediates the slow mGluR1 Ca^{2+} influx (Canepari et al., 2001; Canepari et al., 2004). This channel has been identified as the C3-type transient receptor potential (TRPC3) since in mutant mice lacking this channel all signals associated with the mGluR1-activated non-selective cation conductance are absent (Hartmann et al., 2008). This mouse, as well as another mouse model carrying a point mutation in the TRPC3 channel (Becker et al., 2009), exhibit severe changes in behavioural cerebellar functions. More recently, it was shown that mGluR1s can also activate GluD2 delta "orphan" glutamate receptors, raising the question of whether the mGluR1-activated non-selective cation conductance is actually composed by different channels (Ady et al., 2008). Notably, critical mutations of GluRD2 impair synaptic plasticity and motor learning and cerebellar behavioral functions (Hirano, 2006). Regardless of the identity of the channel underlying the slow mGluR1 Ca^{2+} influx, in this study we report a clear role for this conductance. During the time window of mGluR1 action, Ca^{2+} entering the cell after a PF-EPSP burst binds to mobile proteins forming the rich endogenous buffer of PNs (Bastianelli, 2003). Therefore, in this critical time window, the buffer capacity of PN dendrites, which is exceptionally high at rest (Fierro and Llano, 1996), can locally lower to a level that enables Ca^{2+} influx associated with a CF-EPSP to activate molecular pathways that would not be activated by an unpaired CF-EPSP. The transient saturation of the endogenous buffer has been already identified as crucial computational element that allows local integration of Ca^{2+} signals (Maeda et al., 1999). However, experimental evidence of endogenous buffer saturation was associated with dendritic depolarisation (Canepari and Vogt, 2008), co-localised with activated VGCCs which go beyond the spatial pattern of activated spines. In contrast, endogenous buffer saturation caused by the slow Ca^{2+} influx can be segregated to activated synapses. In general, the spatial pattern of activated spines (Schmidt et al., 2007) and their geometry (Schmidt and Eilers, 2009) are expected to be determinants of endogenous buffer saturation in the case of synaptic Ca^{2+} influx. Finally, endogenous buffer saturation caused by the slow mGluR1 Ca^{2+} influx is likely co-localising with the potentiated T-type VGCCs when the dendrite is at *hyp* state, since the two mGluR1-mediated mechanisms share the same molecular pathway (Hildebrand et al., 2009).

Perspectives

This study was achieved by monitoring fluorescence simultaneously in large portions of PN dendrites with a spatial resolution of ~10 µM. Thus, the dendritic sites of recording comprise several spines and the parent dendritic segment. A full understanding of the signals in terms of individual spines and dendritic bulks, which is not available in this study, should be achieved in the near future either by reducing the temporal resolution using rapid multisite confocal imaging (Filipis et al., 2018), or by reducing the number of recording spots using 2-photon random access microscopy (Otsu et al., 2008). A second question that should be explored in detail is the relation between the initial V_m state and the induction of PF synaptic

plasticity. Numerous studies have investigated other parameters as crucial determinants of PF synaptic plasticity, including timing, size of Ca^{2+} signals, spatial arrangements of synaptic inputs and others (Vogt and Canepari, 2010). In this study we show that a scenario, where a specific Ca^{2+} source (the T-type VGCC) is locally boosted and amplified by mGluR1s, occurs only when the initial initial V_m is hyperpolarised, a phenomenon that can translate into an important information processing rule associated with cerebellar function.

References

Ady V, Perroy J, Tricoire L, Piochon C, Dadak S, Chen X, Dusart I, Fagni L, Lambolez B, Levenes C (2014) Type 1 metabotropic glutamate receptors (mGlu1) trigger the gating of GluD2 delta glutamate receptors. EMBO Rep 15:103-109.

Ait Ouares K, Filipis L, Tzilivaki A, Poirazi P, Canepari M (2019) Two Distinct Sets of Ca_{2+} and K_{+} Channels Are Activated at Different Membrane Potentials by the Climbing Fiber Synaptic Potential in Purkinje Neuron Dendrites. J Neurosci 39:1969-1981.

Ait Ouares, K, Jaafari, N, Canepari, M (2016) A generalised method to estimate the kinetics of fast Ca(2+) currents from Ca(2+) imaging experiments. J Neurosci Methods 268:66 -77.

Ascher P, Nowak L (1987) Electrophysiological studies of NMDA receptors. Trends Neurosci 10:284-288.

Bastianelli E (2003) Distribution of calcium-binding proteins in the cerebellum. Cerebellum 2:242-262.

Becker EB, Oliver PL, Glitsch MD, Banks GT, Achilli F, Hardy A, Nolan PM, Fisher EM, Davies KE (2009) A point mutation in TRPC3 causes abnormal Purkinje cell development and cerebellar ataxia in moonwalker mice. Proc Natl Acad Sci USA 106:6706-6711.

Bouvier G, Aljadeff J, Clopath C, Bimbard C, Ranft J, Blot A, Nadal JP, Brunel N, Hakim V, Barbour B (2018) Cerebellar learning using perturbations. Elife 7:pii e31599.

Bower JM (2002) The organization of cerebellar cortical circuitry revisited: implications for function. Ann N Y Acad Sci 978:135-155.

Brenowitz SD, Regehr WG (2005) Associative short-term synaptic plasticity mediated by endocannabinoids. Neuron 45:419–431.

Canepari M, Auger C, Ogden D (2004) Ca2+ ion permeability and single-channel properties of the metabotropic slow EPSC of rat Purkinje neurons. J Neurosci 24:3563–3573.

Canepari M, Mammano F (1999) Imaging neuronal calcium fluorescence at high spatio-temporal resolution. J Neurosci Methods 87:1-11.

Canepari M, Papageorgiou G, Corrie JET, Watkins C, Ogden D (2001) The conductance underlying the parallel fibre slow EPSP in rat cerebellar Purkinje neurones studied with photolytic release of l-glutamate. J Physiol 533:765–772.

Canepari M, Ogden D (2003) Evidence for protein tyrosine phosphatase, tyrosine kinase, G-protein regulation of the parallel fiber metabotropic slow EPSC of rat cerebellar Purkinje neurons. J Neurosci 23:4066–4071.

Canepari M, Ogden D (2006) Kinetic, pharmacological and activity-dependent separation of two Ca2+ signalling pathways mediated by type 1 metabotropic glutamate receptors in rat Purkinje neurones. J Physiol 573:65–82.

Canepari M, Vogt KE (2008) Dendritic spike saturation of endogenous calcium buffer and induction of postsynaptic cerebellar LTP. PLoS ONE 3:e4011.

Canepari M, Willadt S, Zecevic D, Vogt KE (2010) Imaging Inhibitory Synaptic Potentials Using Voltage Sensitive Dyes. Biophys J 98:2032-2040.

Debanne D (1996) Associative synaptic plasticity in hippocampus and visual cortex: cellular mechanisms and functional implications. Rev Neurosci 7:29-46.

Fierro L, Llano I (1996) High endogenous calcium buffering in Purkinje cells from rat cerebellar slices. J Physiol 496:617–625.

Filipis L, Ait Ouares K, Moreau P, Tanese D, Zampini V, Latini A, Bleau C, Bleau C, Graham J, Canepari M (2018) A novel multisite confocal system for rapid Ca2+ imaging from submicron structures in brain slices. J Biophotonics:11(3).

Finch EA, Augustine GJ (1998) Local calcium signalling by inositol-1,4,5-trisphosphate in Purkinje cell dendrites. Nature 396:753-756.

Gaffield MA, Rowan MJM, Amat SB, Hirai H, Christie JM (2018) Inhibition gates supralinear Ca_{2+} signaling in Purkinje cell dendrites during practiced movements. Elife 7:pii e36246.

Hartmann J, Dragicevic E, Adelsberger H, Henning HA, Sumser M, Abramowitz J, Blum R, Dietrich A, Freichel M, Flockerzi V, Birnbaumer L, Konnerth A (2008) TRPC3 channels are required for synaptic transmission and motor coordination. Neuron 59:392-398.

Hartell NA (1994) Induction of cerebellar long-term depression requires activation of glutamate metabotropic receptors. Neuroreport 14:913-916.

Hartell NA (2002) Parallel fiber plasticity. Cerebellum 1:3-18.

Hildebrand ME, Isope P, Miyazaki T, Nakaya T, Garcia E, Feltz A, Schneider T, Hescheler J, Kano M, Sakimura K, Watanabe M, Dieudonné S, Snutch TP (2009) Functional coupling between mGluR1 and Cav3.1 T-type calcium channels contributes to parallel fiber-induced fast calcium signaling within Purkinje cell dendritic spines. J Neurosci 29:9668-9682.

Hirano T (2006) Cerebellar regulation mechanisms learned from studies on GluRdelta2. Mol Neurobiol 33:1-16.

Hyrc KL, Bownik JM, Goldberg MP (2000) Ionic selectivity of low-affinity ratiometric calcium indicators: mag-Fura-2, Fura-2FF and BTC. Cell Calcium 27:75-86.

Isope P, Hildebrand ME, Snutch TP (2012) Contributions of T-type voltage-gated calcium channels to postsynaptic calcium signaling within Purkinje neurons. Cerebellum 11:651-665.

Ito M (2001) Cerebellar long-term depression: characterization, signal transduction, functional roles. Physiol Rev 81:1143-1195.

Jaafari N, Canepari M (2016) Functional coupling of diverse voltage-gated Ca(2+) channels underlies high fidelity of fast dendritic Ca(2+) signals during burst firing. J Physiol 594:967-983.

Jaafari N, De Waard M, Canepari M (2014) Imaging Fast Calcium Currents beyond the Limitations of Electrode Techniques. Biophys J 107:1280-1288.

Jaafari N, Marret E, Canepari M (2015) Using simultaneous voltage and calcium imaging to study fast Ca2+ channels. Neurophotonics 2:021010.

Jörntell H, Hansel C (2006) Synaptic memories upside down: bidirectional plasticity at cerebellar parallel fiber-Purkinje cell synapses. Neuron 52:227-238.

Kano M, Garaschuk O, Verkhratsky A, Konnerth, A (1995) Ryanodine receptor-mediated intracellular calcium release in rat cerebellar Purkinje neurones. J Physiol 487:1-16.

Kim SJ, Jin Y, Kim J, Shin JH, Worley PF, Linden DJ (2008) Transient upregulation of postsynaptic IP3-gated Ca release underlies short-term potentiation of metabotropic glutamate receptor 1 signaling in cerebellar Purkinje cells. J Neurosci 28:4350-4355.

Kitamura K, Häusser M (2011) Dendritic calcium signaling triggered by spontaneous and sensory-evoked climbing fiber input to cerebellar Purkinje cells in vivo. J Neurosci 31:10847-10858.

Knöpfel T, Vranesic I, Staub C, Gähwiler BH (1991) Climbing Fibre Responses in Olivo-cerebellar Slice Cultures. II. Dynamics of Cytosolic Calcium in Purkinje Cells. Eur J Neurosci 3:343-348.

Kosaka T, Kosaka K, Nakayama T, Hunziker W, Heizmann CW (1993). Axons and axon terminals of cerebellar Purkinje cells and basket cells have higher levels of parvalbumin immunoreactivity than somata and dendrites: quantitative analysis by immunogold labeling. Exp Brain Res 93:483–491.

Maeda H, Ellis-Davies GC, Ito K, Miyashita, Y Kasai H (1999) Supralinear Ca2+ signaling by cooperative and mobile Ca2+ buffering in Purkinje neurons. Neuron 24:989–1002.

Maejima T, Oka S, Hashimotodani Y, Ohno-Shosaku T, Aiba A, Wu D, Waku K, Sugiura T, Kano M (2005). Synaptically driven endocannabinoid release requires Ca2+-assisted metabotropic glutamate receptor subtype 1 to phospholipase Cbeta4 signaling cascade in the cerebellum. J Neurosci 25:6826–6835.

Miyakawa H, Lev-Ram V, Lasser-Ross, N, Ross WN (1992). Calcium transients evoked by climbing fiber and parallel fiber synaptic inputs in guinea pig cerebellar Purkinje neurons. J Neurophysiol 68:1178-1189.

Nägerl UV, Novo D, Mody I, Vergara JL (2000) Binding kinetics of calbindin-D(28k) determined by flash photolysis of caged Ca(2+). Biophys J 79:3009-3018.

Otsu Y, Bormuth V, Wong J, Mathieu B, Dugué GP, Feltz A, Dieudonné S (2008) Optical monitoring of neuronal activity at high frame rate with a digital random-access multiphoton (RAMP) microscope. J Neurosci Methods 173:259-270.

Otsu Y, Marcaggi P, Feltz A, Isope P, Kollo M, Nusser Z, Mathieu B, Kano M, Tsujita M, Sakimura K, Dieudonné S (2014) Activity-dependent gating of calcium spikes by A-type K+ channels controls climbing fiber signaling in Purkinje cell dendrites. Neuron 84:137–151.

Roome CG, Kuhn B (2018) Simultaneous dendritic voltage and calcium imaging and somatic recording from Purkinje neurons in awake mice. Nat Commun 9:3388.

Rowan MJM, Bonnan A, Zhang K, Amat SB, Kikuchi C, Taniguchi H, Augustine GJ, Christie JM (2018) Graded Control of Climbing-Fiber-Mediated Plasticity and Learning by Inhibition in the Cerebellum. Neuron 99:999-1015.

Safo PK, Regehr WG (2005) Endocannabinoids control the induction of cerebellar LTD. Neuron 48:647–659.

Safo PK, Regehr WG (2008) Timing dependence of the induction of cerebellar LTD. Neuropharmacology 54:213-218.

Savitzky A, Golay JE (1964) Smoothing and differentiation of data by simplified least squares procedures. Anal Chem 36:1627–1639.

Schmidt H, Eilers J (2009) Spine neck geometry determines spino-dendritic cross-talk in the presence of mobile endogenous calcium binding proteins. J Comput Neurosci 27:229-243.

Schmidt H, Kunerth S, Wilms C, Strotmann R, Eilers J (2007) Spino-dendritic cross-talk in rodent Purkinje neurons mediated by endogenous Ca2+-binding proteins. J Physiol 581:619-629.

Suvrathan A, Raymond JL (2018) Depressed by Learning-Heterogeneity of the Plasticity Rules at Parallel Fiber Synapses onto Purkinje Cells. Cerebellum 17:747-755.

Takechi H, Eilers J, Konnerth A (1998) A new class of synaptic response involving calcium release in dendritic spines. Nature 396:757–760.

Tempia F, Alojado ME, Strata P, Knöpfel T (2001) Characterization of the mGluR(1)-mediated electrical and calcium signaling in Purkinje cells of mouse cerebellar slices. J Neurophysiol 86:1389-1397.

Vogt KE, Canepari M (2010) On the induction of postsynaptic granule cell-Purkinje neuron LTP and LTD. Cerebellum 9:284–290.

Vogt KE, Gerharz S, Graham J, Canepari M (2011a) High-resolution simultaneous voltage and Ca^{2+} imaging. J Physiol 589:489–494.

Vogt KE, Gerharz S, Graham J, Canepari M (2011b) Combining membrane potential imaging with L-glutamate or GABA photorelease. PLoS ONE 6:e24911.

Wang SS, Denk W, Hausser M (2000). Coincidence detection in single dendritic spines mediated by calcium release. Nat Neurosci 3:1266–1273.

Zoukimian C, Meudal H, De Waard S, Ait Ouares K, Nicolas S, Canepari M, Béroud R, Landon C, De Waard M, Boturyn D (2019) Synthesis by native chemical ligation and characterization of the scorpion toxin AmmTx3. Bioorg Med Chem 27:247-253.

Figure Legend

Figure 1. Timing and localisation of supralinear Ca^{2+} signals. ***A***, Reconstruction of PN filled with 2 mM OG5N (left) with position of two stimulating electrodes for the CF and PFs and two regions of interest indicated (*R1* and *R2*). Somatic V_m and Ca^{2+} $\Delta F/F_0$ signals at *R1* and *R2* associated PFs stimulated with 5 pulses at 100 Hz with timing indicated by purple lines (right). Spatial distribution of $\Delta F/F_0$ signal corresponding to the 2^{nd}-5^{th} PF-EPSPs and to the peak of the slow Ca^{2+} signal depicted using a colour code. ***B***, Somatic V_m and Ca^{2+} $\Delta F/F_0$ signals at *R1* and *R2* associated with CF stimulation unpaired (light blue traces) or paired (dark blue traces) with PF stimulation at 100 Hz (timing indicated by purple lines) following at 60 ms, 100 ms or 150 ms from the first PF pulse (timing indicated by purple triangle). Spatial distribution of the $\Delta F/F_0$ signal associated with CF-EPSP paired with PF stimulation depicted using a colour code. ***C***, Ca^{2+} $\Delta F/F_0$ signals at *R1* associated with CF stimulation unpaired or paired with PF stimulation delayed by 60 ms, 100 ms or 150 ms from the first PF pulse in control solution (blue traces) or after addition of 20 µM of the mGluR1 antagonist CPCCOEt (green traces). The time window outlined is reported below. ***D***, Mean ± SD (N = 6 cells) of $\Delta F/F_0$ ratio between the paired and unpaired signals in control solution or after addition of CPCCOEt. "*" indicates significant inhibition of supralinear Ca^{2+} signal by CPCCOEt ($p< 0.01$, paired t-test). The dotted line depicts $\Delta F/F_0$ ratio = 1. All optical signals were from averages of 4 trials.

Figure 2. Supralinear Ca^{2+} signals at different initial V_m. ***A***, Reconstruction of PN filled with 2 mM OG5N (left) with position of two stimulating electrodes for the CF and PFs and a region of interest adjacent to the PF stimulating electrode indicated. ***B***, Somatic V_m and Ca^{2+} $\Delta F/F_0$ signals at the region of interest associated with CF stimulation unpaired (light blue traces) or paired (dark blue traces) with PF stimulation (timing indicated by purple lines) delayed by 110 ms from the first PF pulse (timing indicated by purple triangle) in the case of hyperpolarised (*hyp*, ~-80 mV) or V_{rest} (*rest*, ~-60 mV). Spatial distribution of the $\Delta F/F_0$ signal associated with CF-EPSP paired with PF stimulation depicted using a colour code. ***C***, Same Ca^{2+} $\Delta F/F_0$ signals associated with CF stimulation unpaired or paired with PF stimulation in control solution (blue traces) or after addition of 20 µM of the mGluR1 antagonist CPCCOEt (green traces). The time window outlined is reported below. ***D***, Mean ± SD (N = 6 cells) of the $\Delta F/F_0$ ratio between the paired and unpaired signals in control solution or after addition of CPCCOEt. "*" indicates a significant inhibition of supralinear Ca^{2+} signal by CPCCOEt ($p< 0.01$, paired t-test). The dotted line depicts $\Delta F/F_0$ ratio = 1. All optical signals were from averages of 4 trials.

Figure 3. Kinetics of supralinear Ca^{2+} signals. ***A***, Reconstruction of PN filled with 2 mM OG5N; position of PF stimulating electrode and adjacent region of interest indicated. Somatic V_m and Ca^{2+} $\Delta F/F_0$ signals in the region of interest associated with different protocols: from left to right a CF-EPSP unpaired at *hyp* and *rest* states, paired with a PF-EPSPs train delayed by 110 ms from the first PF stimulus at *hyp* and *rest* states, and paired with a PF-EPSPs train delayed by 60 ms from the first PF stimulus. On the bottom, V_m

and Ca^{2+} signals associated with the CF-EPSP from the 9 individual trials used for the averages aligned and displayed on a 3 ms time window, to show that single acquisitions are not affected by jitters. ***B***, On the left, Ca^{2+} $\Delta F/F_0$ signals associated with the CF-EPSP reported in panel *A* aligned with the CF stimulation (dotted line indicated with "*stim*") on a time window of 5 ms; on the right, same signals smoothed by a 20-points Savitsky-Golay filter and normalised to the peak on a time window of 3 ms. Traces are reported twice, first superimposed to the signal corresponding to the unpaired CF at *hyp* state and second to the signal corresponding to the unpaired CF at *rest* state. ***C***, Normalised time derivative ($d(\Delta F/F_0)/dt$) of the filtered signals in panel B. Traces are reported twice, first superimposed to the time derivative corresponding to the unpaired CF at *hyp* state and second to the time derivative corresponding to the unpaired CF at *rest* state. The two dotted lines indicate the time of the peak of the $d(\Delta F/F_0)/dt$ signals. Δt_{peak} indicates the time difference between the two peaks for unpaired CF at *hyp* state and at *rest* state. ***D***, Mean ± SD (N = 8 cells) of Δt_{peak} expressed in samples from the signal associated with the unpaired CF at *hyp* state (top) and from the signal associated with the unpaired CF at *rest* state (bottom). "*" indicates a significant difference from the signal of reference ($p < 0.01$, paired t-test). All optical signals were from averages of 9 trials.

Figure 4. Supralinear Ca^{2+} signals in the presence of heparin or ryanodine. ***A***, Reconstruction of PN filled with 2 mM OG5N and 1 mg/mL of heparin sodium salt to block InsP3 receptors (left); position of PF stimulating electrode and adjacent region of interest indicated. Somatic V_m and Ca^{2+} $\Delta F/F_0$ signals in the region of interest associated with different protocols: from left to right a CF-EPSP unpaired at *hyp* and *rest* states, paired with a PF-EPSPs train delayed by 110 ms from the first PF stimulus at *hyp* and *rest* states, and paired with a PF-EPSPs train delayed by 60 ms from the first PF stimulus. ***B***, Same as *A*, but with the internal solution containing 100 µM ryanodine to block ryanodine receptors. ***C***, Mean ± SD (N = 6 cells for each group) of $\Delta F/F_0$ ratio between the paired and unpaired signals in the presence of heparin (green columns) or ryanodine (purple columns). Blue columns are mean ± SD of $\Delta F/F_0$ ratios in control conditions already reported in Fig. 1 and Fig. 2. Values for heparin were: 3.17 ± 0.41 for 110 ms CF delay at *hyp* states; 2.02 ± 0.27 for 110 ms CF delay at *rest* states; 2.72 ± 0.54 for 60 ms CF delay. Values for ryanodine were: 3.06 ± 0.85 for 110 ms CF delay at *hyp* states; 1.93 ± 0.56 for 110 ms CF delay at *rest* states; 2.56 ± 0.80 for 60 ms CF delay. Experiments were performed 45 minutes after whole cell to obtain full equilibration of the internal solution. Used concentrations of heparin and ryanodine were the maximal tolerated by the cells for one-hour recording. All optical signals were from averages of 4 trials.

Figure 5. Dendritic V_m associated with mGluR1-independent supralinear Ca^{2+} signals. ***A***, Dendrite of PN filled with the voltage-sensitive dye JPW1114 (left); position of PF stimulating electrode and adjacent region of interest indicated. Somatic (top) and dendritic (bottom) V_m in the region of interest associated with a CF-EPSP unpaired or paired with a PF-EPSPs train with the CF stimulation delayed by 60 ms from the first PF stimulus. ***B***, On a time window of 20 ms, dendritic V_m signals of panel *A*. V_{init} and V_{peak} indicate the initial and peak V_m calibrated in mV. ***C***, Mean ± SD (N = 8 cells) of V_{init} and V_{peak} for the signals associated with an unpaired CF-EPSP (-83 ± 3 mV and -18 ± 5 mV respectively) and for the signals

associated with a CF-EPSP paired with a PF-EPSPs train with the CF stimulation delayed by 60 ms from the first PF stimulus (-61 ± 4 mV and -5 ± 2 mV respectively). "*" indicates significant differences of V_{init} and V_{peak} ($p < 0.01$, paired t-test). All optical signals were from averages of 4 trials.

Figure 6. Dendritic V_m transients associated with mGluR1-dependent supralinear Ca^{2+} signals. ***A***, Dendritic PN area filled with the VSD JPW1114 and 1 mM Fura-2FF (left); position of PF stimulating electrode and two regions of interest (*R1* and *R2*) indicated. Somatic V_m and Fura-2FF $-\Delta F/F_0$ signals (right) from single trials at *R1* and *R2* associated with CF stimulation unpaired (light blue traces) or paired (dark blue traces) with PF stimulation in the case of *hyp* (~-80 mV) or *rest* (~-60 mV) initial V_m, indicating supralinear Ca^{2+} signals at *R1*. ***B***, V_m calibrated recordings associated with CF stimulation unpaired (red traces) or paired (pink traces) with PF stimulation at *R1* and *R2* superimposed to somatic V_m, in the case of *hyp* or *rest* initial V_m. ***C***, V_m recordings at *R1* shown in panel *B* filtered as following: for the unpaired CF, average of the signals before the CF stimulation and in the next 20 ms a 4-points median filter is applied; for the paired CF, a 64-points median filter is applied after the PF train and before the CF stimulation and in the next 20 ms a 4-points median filter is applied. ***D***, Same signals of panel *C* in the outlined time window; the values of the V_m transients are indicated. ***E***, Mean ± SD (N = 7 cells) of the V_m transient difference between the paired and unpaired CF in the case of *hyp* or *rest* initial V_m. "*" indicates a significant difference ($p < 0.01$, paired t-test). All optical signals were from averages of 4 trials.

Figure 7. Computer simulations of the Ca^{2+} fluorescence signals in the presence of 2 mM OG5N and 400 µM Fura-2. ***A***, Ca^{2+} influx used in the computer simulations associated with a CF-EPSP: Gaussian function of 15 µM/ms (left) or 20 µM/ms (right) and 1.5 ms time constant unpaired or paired with a preceding slow Ca^{2+} influx approximated by another Gaussian function of 4 µM/ms and 45 ms time constant. ***B***, Computer simulations of the putative OG5N $\Delta F/F_0$ signal in the absence of Fura2 using the model described in detail in the Materials and Methods and the Ca^{2+} influx reported in panel A. The $\Delta F/F_0$ signal was extrapolated from the Ca^{2+} bound to the indicator using the dynamic range of 15 measured in Ait Ouares et al (2016). ***C***, Computer simulations of the putative OG5N $\Delta F/F_0$ signal (top) and of the putative Fura2 $-\Delta F/F_0$ signal (bottom) in the presence of 400 µM Fura2 using the same model and Ca^{2+} influx as in panel B. The Fura2 $-\Delta F/F_0$ signal was extrapolated from the Ca^{2+} bound to the indicator using the dynamic range of 0.9 used in Ait Ouares et al (2019). The values of the variable *S*, described in detail in the *Experimental design and statistical analysis* section of the Materials and Methods are reported for the two indicators.

Figure 8. Contribution of saturation of endogenous Ca^{2+} buffers to supralinear Ca^{2+} signals. ***A***, Dendritic PN area filled with two Ca^{2+} indicators (left): OG5N (2 mM, K_D = 35 µM) and Fura2 (0.4 mM, K_D = 0.2 µM); position of PF stimulating electrode and adjacent region of interest indicated. Somatic V_m and Ca^{2+} signals in the region of interest associated with different protocols: from left to right a CF-EPSP unpaired at *hyp* and *rest* states, paired with a PF-EPSPs train delayed by 110 ms from the first PF stimulus at *hyp* and *rest* states, and paired with a PF-EPSPs train delayed by 60 ms from the first PF stimulus; signals from the two

indicators (OG5N $\Delta F/F_0$ and Fura -$\Delta F/F_0$) were obtained by alternating the excitation wavelength. ***B***, Same Ca^{2+} transients associated with the CF-EPSP in panel *A*, for the two indicators, superimposed either to the unpaired CF transient at *hyp* state or to the unpaired CF transient at *rest* state. ***C***, *S* is defined as the ratio between the $\Delta F/F_0$ peaks for each protocol and the $\Delta F/F_0$ peak associated with the unpaired CF stimulation. On the left, mean ± SD (N = 8 cells) of *S* corresponding to Fura2 signals (S_{Fura2}) in the different cases as reported in the legend; "*" indicates a significant difference ($p< 0.01$, paired t-test) between the two $\Delta F/F_0$ peaks used to calculate S_{Fura2}. On the right, mean ± SD (N = 8 cells) of S_{Fura2}/S_{OG5N} in the different cases as reported in the legend; "*" indicates a significant difference ($p< 0.01$, paired t-test) between S_{OG5N} and S_{Fura2}. "**" indicates a significant difference ($p< 0.01$, paired t-test) between two S_{OG5N}/S_{Fura2} ratios. All optical signals were from averages of 4 trials.

Figure 9. Supralinear Ca^{2+} signals after blocking T-type VGCCs. ***A***, Dendritic area of a PN filled with 2 mM OG5N (left) with position of PF stimulating electrode and an adjacent region of interest indicated. On the right, somatic V_m (black traces) and Ca^{2+} $\Delta F/F_0$ (blue or green traces) signals at the region of interest associated with CF stimulation unpaired (light traces) or paired (dark traces) with PF stimulation (timing indicated by purple lines) delayed by 110 ms from the first PF pulse (timing indicated by purple triangle) in the case of *hyp* or *rest* initial V_m. Signals were acquired in control conditions (blue traces) or after addition of 30 µM of the T-type VGCC blocker NNC (green traces). ***B***, Same Ca^{2+} signals in panel *A* over a 20 ms time window outlined. ***C***, Mean ± SD (N = 6 cells) of the ratios between the $\Delta F/F_0$ peak after addition of NNC and the peak under control condition; dark blue columns are for paired signals; light blue columns are for unpaired CF signals. Ratios are calculated both for unpaired and paired CF signals. "*" indicates a significant reduction of paired Ca^{2+} signal after addition of NNC ($p< 0.01$, paired t-test). The dotted line depicts the ratio = 1. All optical signals were from averages of 4 trials.

Figure 10. Use- dependent block of mGluR1 slow Ca^{2+} transients and of supralinear Ca^{2+} signals. ***A***, Dendritic area of a PN filled with 2 mM OG5N (left) with position of PF stimulating electrode and an adjacent region of interest indicated. Somatic V_m and Ca^{2+} $\Delta F/F_0$ signals at the region of interest associated with an unpaired CF-EPSP, with PFs stimulated with 5 pulses at 100 Hz or with a CF-EPSP paired with PF stimulation at *hyp* state. Black and dark blue traces were from recordings in control solution. Traces at different gray or blue tones were from recordings performed a time (t) after addition of 250 µM of the channel blocker IEM1460. ***B***, On the left, same recordings in *A* for PF stimulation only (*PF*) in control condition and 20 minutes after addition of IEM1460; the exponential "*fit*" of the Ca^{2+} $\Delta F/F_0$ decay after the 5^{th} PF-EPSP is also reported with a dotted line. On the right, Ca^{2+} transients associated with the slow mGluR1-mediated component calculated as the difference between the Ca^{2+} $\Delta F/F_0$ signals associated with PF stimulation and the *fit* trace on the left. ***C***, Mean ± SD (N = 6 cells) of the ratio between the slow mGluR1-dependent PF-mediated Ca^{2+} transients (*PF* - *fit*) 20 minutes after addition of IEM1460 and in control condition. "*" indicates a significant reduction of the signal ($p< 0.01$, paired t-test). The dotted line depicts the ratio = 1. ***D***, Mean ± SD of the $\Delta F/F_0$ ratio between the paired and unpaired signals in control solution or after addition of IEM1460. "*" indicates a significant inhibition of supralinear Ca^{2+}

signal by IEM1460 ($p< 0.01$, paired t-test). The dotted line depicts $\Delta F/F_0$ ratio = 1. All optical signals were from averages of 4 trials.

Figure 11. Wide mGluR1-dependent supralinear Ca^{2+} signals at *rest* states. ***A***, On the left, dendrite of PN filled with 2 mM OG5N; position of PF stimulating electrode and of two regions of interest indicated (*R1* and *R2*); *R1* is adjacent to the PF stimulating electrode; R2 is ~60 µm away from the PF stimulating electrode. On the right, somatic V_m (top) and dendritic Ca^{2+} signals (bottom) in *R1* and *R2* associated with a CF-EPSP unpaired or paired with a PF-EPSPs train with the CF stimulation delayed by 110 ms from the first PF stimulus at *rest* state. ***B***, On a time window of 20 ms, somatic V_m and dendritic Ca^{2+} signals in *R2* reported in panel A, exhibiting a supralinear Ca^{2+} transient smaller than that in *R1*. ***C***, Somatic V_m (top) and dendritic Ca^{2+} signal associated with an unpaired CF-EPSP in control condition or after addition of the A-type K^+ channel inhibitor AmmTx3. The two supralinear Ca^{2+} signals reported in panels *A* and *B* are qualitatively very similar. All optical signals were from averages of 4 trials.

Figure 12. Supralinear Ca^{2+} signals associated with DHPG application. ***A***, On the left, dendrite of PN filled with 2 mM OG5N (left); a region of interest and the position of a pipette delivering 100 µM DHPG dissolved in external solution are indicated; DHPG application was achieved by applying a 20 ms pulse of pressure using a pressure ejector. On the right, somatic V_m (top) and dendritic Ca^{2+} signals (bottom) in the region of interest associated with a CF-EPSP unpaired (light blue trace) or paired with DHPG application (dark blue trace); the timing of DHPG application and of CF stimulation are indicated with a purple line and a purple arrow respectively; a $\Delta F/F_0$ artefact is observable during the short DHPG application. ***B***, On a time window of 20 ms, dendritic Ca^{2+} signals reported in panel A, exhibiting a supralinear Ca^{2+} transient. ***C***, First on the left, mean ± SD (2.20 ± 0.80, N = 7 cells) of $\Delta F/F_0$ ratio between the CF-associated signal paired with DHPG application and unpaired. Following on the right, mean ± SD of $\Delta F/F_0$ ratios between CF-associated signals paired with PF stimulation and unpaired; the statistics relative to 60 ms delay between the first PF stimulus and the CF stimulation is the same reported in Fig. 1D; the two statistics relative to 110 ms delay between the first PF stimulus and the CF stimulation at *hyp* and *rest* states are the same reported in Fig. 2D. The dotted line depicts $\Delta F/F_0$ ratio = 1.

Figure 13. Illustration of the determinants of the different dendritic supralinear Ca^{2+} signals in PNs. On the top, a representative PN dendritic region indicating the position of the PF stimulation electrode and a hand-drawn schematic dendritic V_m associated with an unpaired CF-EPSP and the consequent Ca^{2+} transient at *hyp* and *rest* states. The V_m transient opens principally T and A channels at the *hyp* state (box *b*), and principally P/Q (and possibly A channels) at the *rest* state (box *a*). In both cases, Ca^{2+} entering through VGCCs binds to the endogenous Ca^{2+} buffer (ECB) without saturating it. On the bottom, a hand-drawn schematic dendritic V_m associated with paired CF-EPSPs and the consequent Ca^{2+} transient. During the PF-EPSPs Ca^{2+} entering through both VGCC types saturates the ECB (box *c*). At 60 ms delay from the first PF-EPSP the CF-Ca^{2+} transient principally mediated by P/Q channels produces a supralinear Ca^{2+} increase because the ECB is saturated (box *d*). At 110 ms delay and at *hyp* state, the CF-Ca^{2+}

transient produces a supralinear Ca^{2+} increase because T channels are potentiated by active mGluR1s and the ECB is saturated by Ca^{2+} entering through the mGluR1-activated channel (box *f*). At 110 ms delay and at *rest* state, the CF-Ca^{2+} transient produces a supralinear Ca^{2+} increase because the ECB is saturated by Ca^{2+} entering through the mGluR1-activated channel and possibly because of a larger Ca^{2+} influx via P/Q channels enhanced by stronger inactivation of A channels by mGluR1s (box *e*).

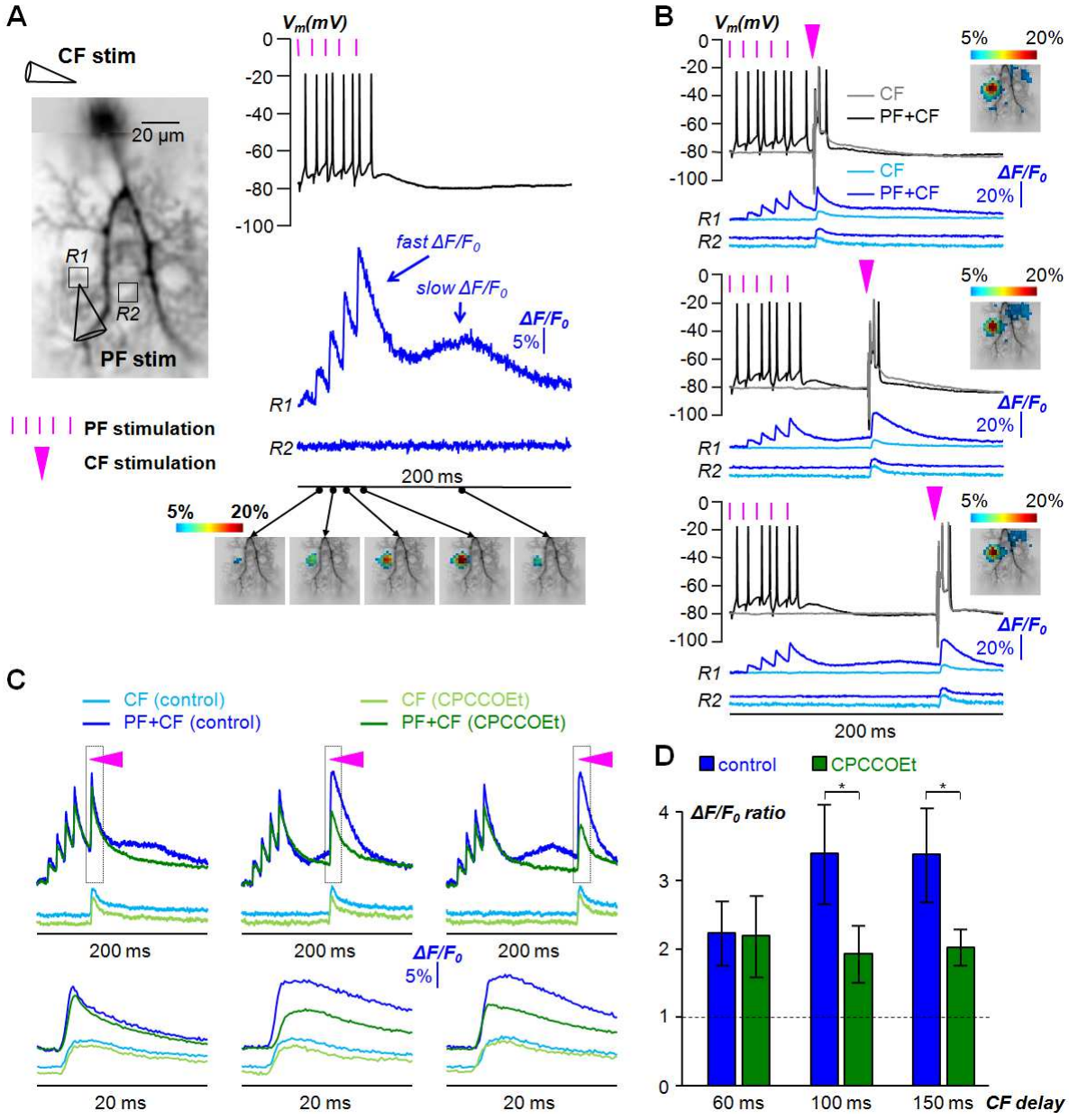
A
CF stim
20 µm
R1
R2
PF stim
PF stimulation
CF stimulation
Vm(mV)
fast ΔF/F0
slow ΔF/F0
ΔF/F0
5%
R1
R2
200 ms
5%
20%
B
Vm(mV)
CF
PF+CF
ΔF/F0
20%
R1
R2
200 ms
C
CF (control)
PF+CF (control)
CF (CPCCOEt)
PF+CF (CPCCOEt)
200 ms
ΔF/F0
5%
20 ms
D
control
CPCCOEt
ΔF/F0 ratio
60 ms
100 ms
150 ms
CF delay

Figure 1

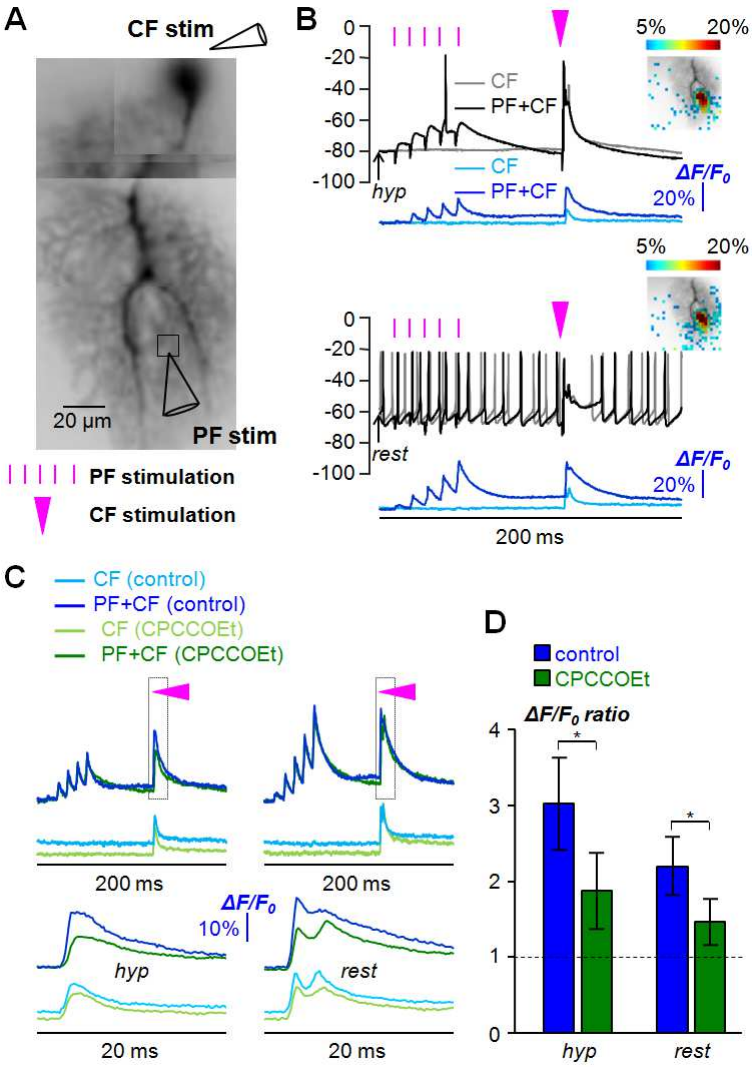
A
CF stim
20 µm
PF stim
PF stimulation
CF stimulation
B
5%
20%
CF
PF+CF
hyp
ΔF/F0
20%
rest
200 ms
C
CF (control)
PF+CF (control)
CF (CPCCOEt)
PF+CF (CPCCOEt)
200 ms
ΔF/F0
10%
hyp
rest
20 ms
D
control
CPCCOEt
ΔF/F0 ratio
hyp
rest

Figure 2

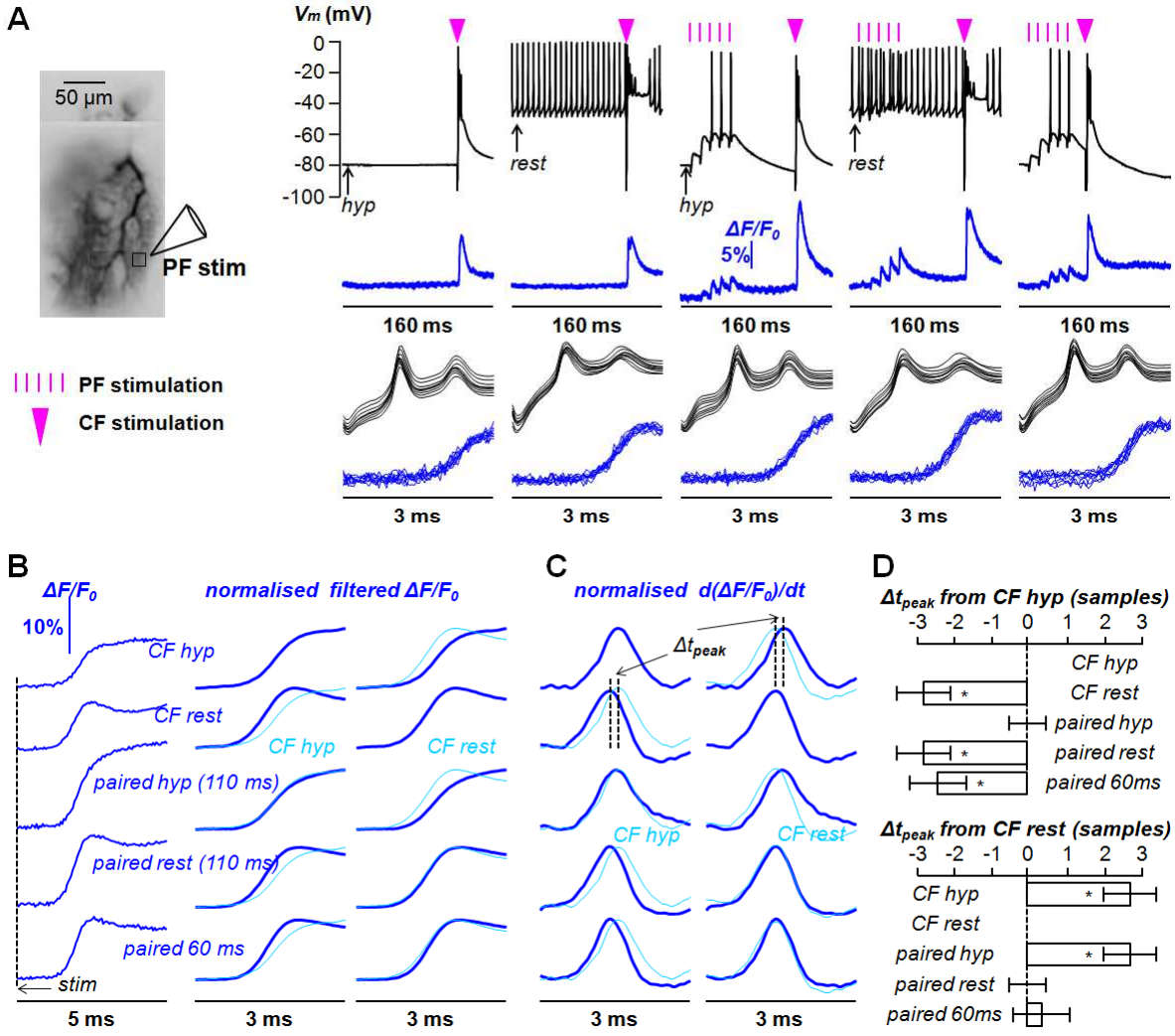
A
50 µm
PF stim
PF stimulation
CF stimulation
Vm (mV)
0
-20
-40
-60
-80
-100
hyp
rest
hyp
rest
ΔF/F0
5%
160 ms
160 ms
160 ms
160 ms
160 ms
3 ms
3 ms
3 ms
3 ms
3 ms
B
ΔF/F0
10%
normalised filtered ΔF/F0
CF hyp
CF rest
paired hyp (110 ms)
paired rest (110 ms)
paired 60 ms
stim
CF hyp
CF rest
5 ms
3 ms
3 ms
C
normalised d(ΔF/F0)/dt
Δtpeak
CF hyp
CF rest
3 ms
3 ms
D
Δtpeak from CF hyp (samples)
-3 -2 -1 0 1 2 3
CF hyp
CF rest
paired hyp
paired rest
paired 60ms
Δtpeak from CF rest (samples)
-3 -2 -1 0 1 2 3
CF hyp
CF rest
paired hyp
paired rest
paired 60ms

Figure 3

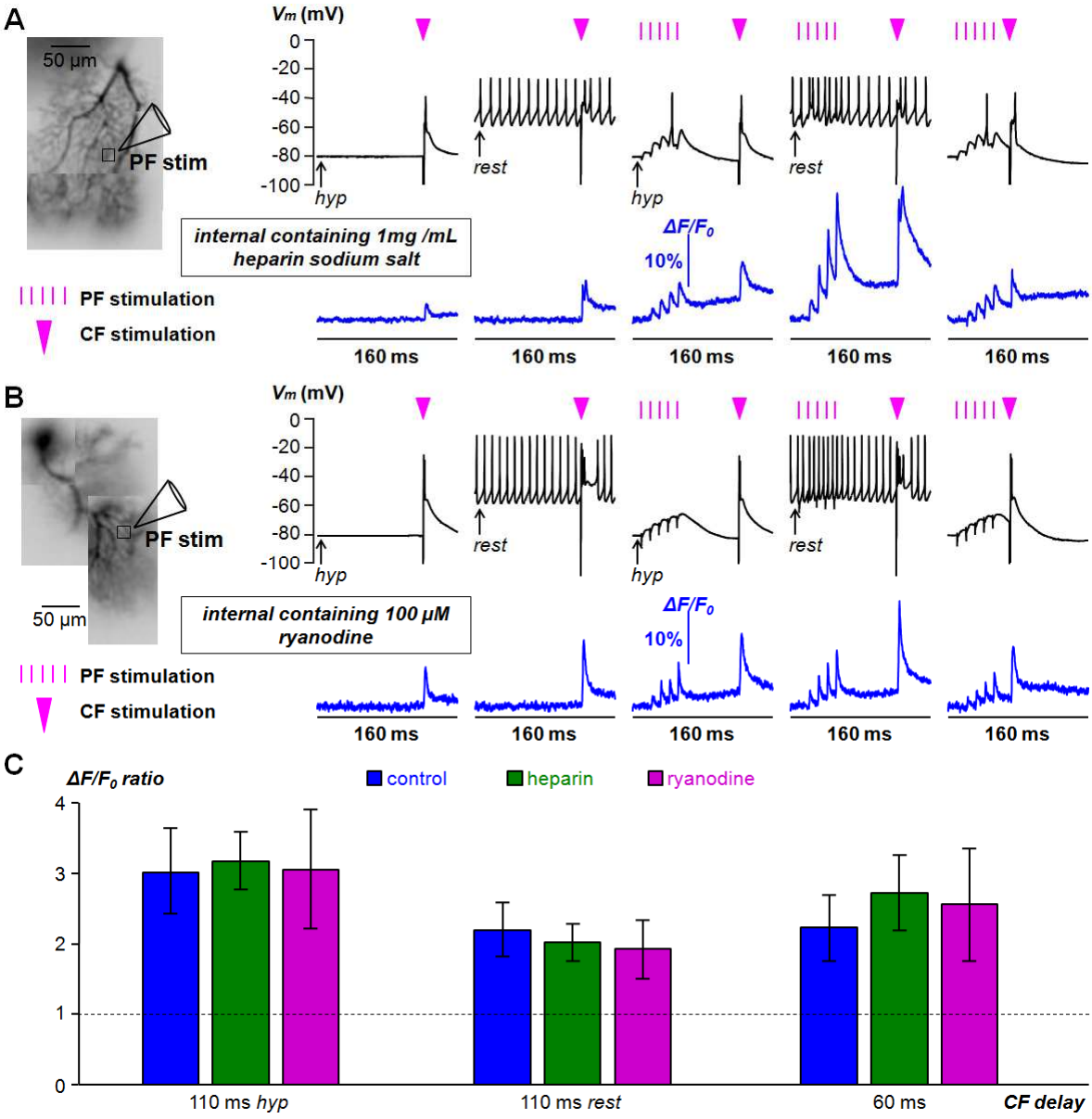
A
50 µm
PF stim
Vm (mV)
0
-20
-40
-60
-80
-100
hyp
rest
internal containing 1mg /mL heparin sodium salt
ΔF/F0
10%
PF stimulation
CF stimulation
160 ms
B
50 µm
PF stim
internal containing 100 µM ryanodine
C
ΔF/F0 ratio
control
heparin
ryanodine
4
3
2
1
0
110 ms hyp
110 ms rest
60 ms
CF delay

Figure 4

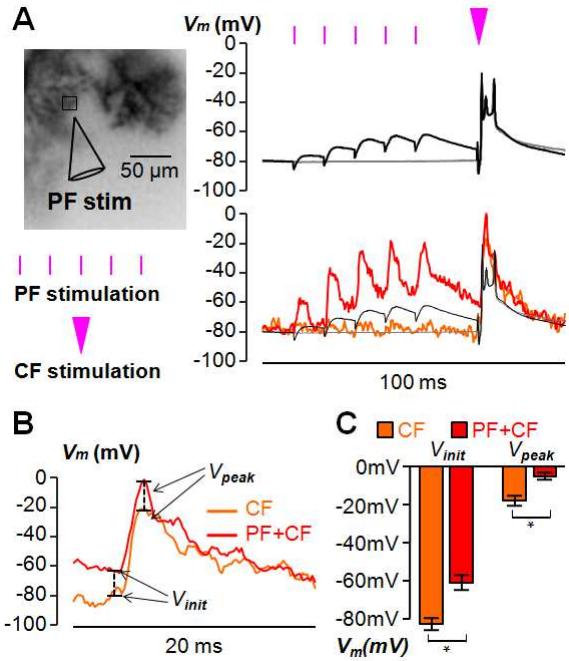
A
Vm (mV)
0
-20
-40
-60
-80
-100
50 μm
PF stim
PF stimulation
CF stimulation
100 ms
B
Vm (mV)
Vpeak
CF
PF+CF
Vinit
20 ms
C
CF
PF+CF
Vinit
Vpeak
0mV
-20mV
-40mV
-60mV
-80mV
Vm(mV)
*
*

Figure 5

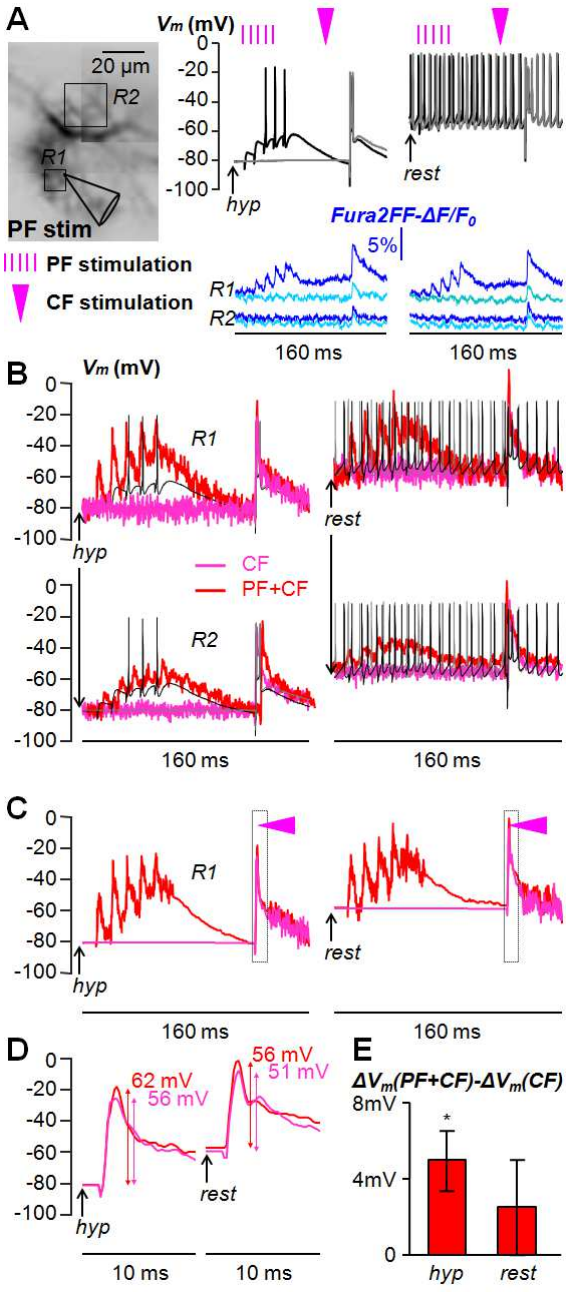
A
Vm (mV)
20 µm
R2
R1
PF stim
PF stimulation
CF stimulation
hyp
rest
Fura2FF-ΔF/F0
5%
R1
R2
160 ms
160 ms
B
Vm (mV)
R1
R2
hyp
rest
CF
PF+CF
160 ms
160 ms
C
R1
hyp
rest
160 ms
160 ms
D
62 mV
56 mV
56 mV
51 mV
hyp
rest
10 ms
10 ms
E
ΔVm(PF+CF)-ΔVm(CF)
8mV
4mV
0
hyp
rest

Figure 6

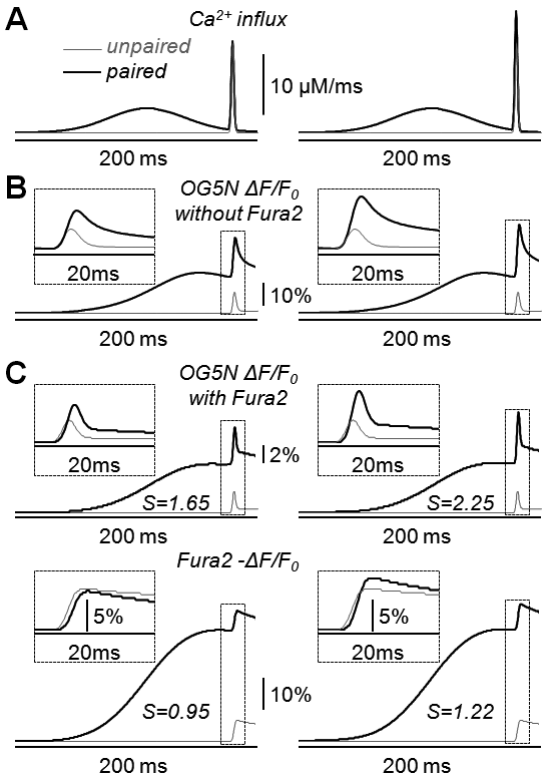
A
Ca2+ influx
unpaired
paired
10 µM/ms
200 ms
200 ms
B
OG5N ΔF/F0
without Fura2
20ms
20ms
10%
200 ms
200 ms
C
OG5N ΔF/F0
with Fura2
20ms
2%
20ms
S=1.65
S=2.25
200 ms
200 ms
Fura2 -ΔF/F0
5%
20ms
5%
20ms
10%
S=0.95
S=1.22
200 ms
200 ms

Figure 7

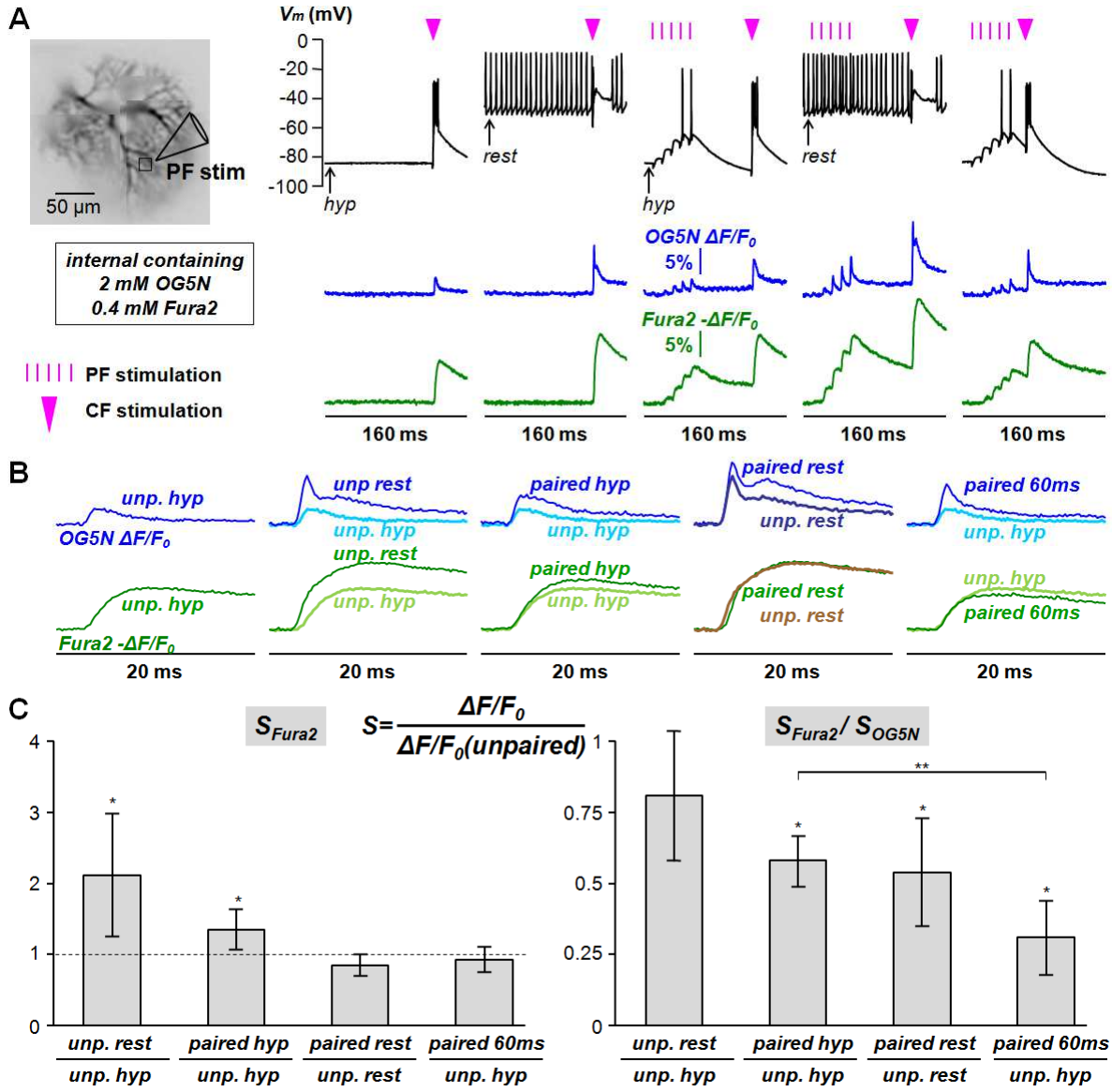
A
Vm (mV)
0
-20
-40
-60
-80
-100
hyp
rest
hyp
rest
PF stim
50 µm
internal containing
2 mM OG5N
0.4 mM Fura2
PF stimulation
CF stimulation
OG5N ΔF/F0
5%
Fura2 -ΔF/F0
5%
160 ms
160 ms
160 ms
160 ms
160 ms
B
unp. hyp
OG5N ΔF/F0
unp rest
unp. hyp
paired hyp
unp. hyp
paired rest
unp. rest
paired 60ms
unp. hyp
unp. hyp
Fura2 -ΔF/F0
unp. rest
unp. hyp
paired hyp
unp. hyp
paired rest
unp. rest
unp. hyp
paired 60ms
20 ms
20 ms
20 ms
20 ms
20 ms
C
SFura2
S=ΔF/F0 / ΔF/F0(unpaired)
SFura2/ SOG5N
4
3
2
1
0
1
0.75
0.5
0.25
0
*
*
*
*
*
*
**
unp. rest
unp. hyp
paired hyp
unp. hyp
paired rest
unp. rest
paired 60ms
unp. hyp
unp. rest
unp. hyp
paired hyp
unp. hyp
paired rest
unp. rest
paired 60ms
unp. hyp

Figure 8

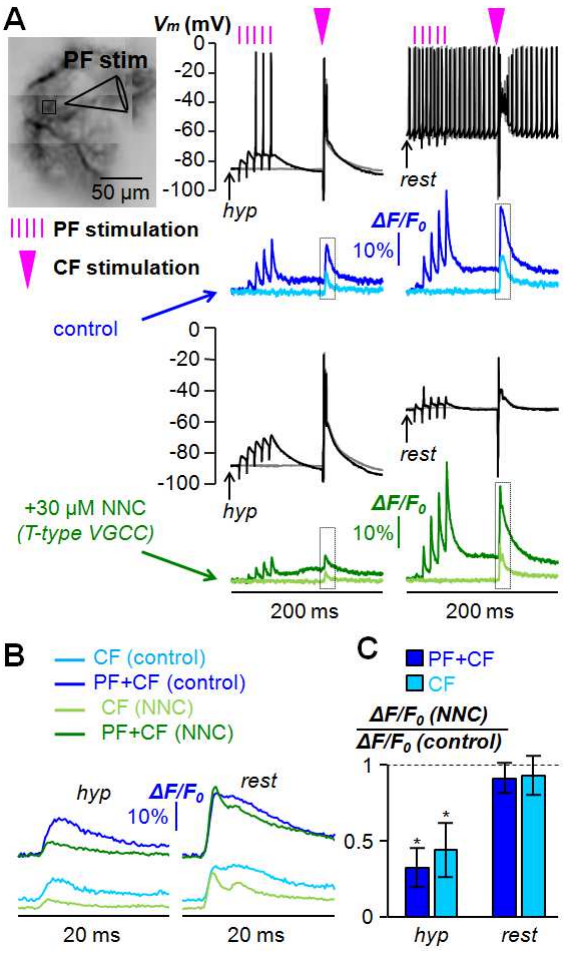
A
Vm (mV)
PF stim
50 µm
PF stimulation
CF stimulation
control
hyp
rest
ΔF/F0
10%
+30 µM NNC
(T-type VGCC)
200 ms
B
CF (control)
PF+CF (control)
CF (NNC)
PF+CF (NNC)
20 ms
C
PF+CF
CF
ΔF/F0 (NNC)
ΔF/F0 (control)

Figure 9

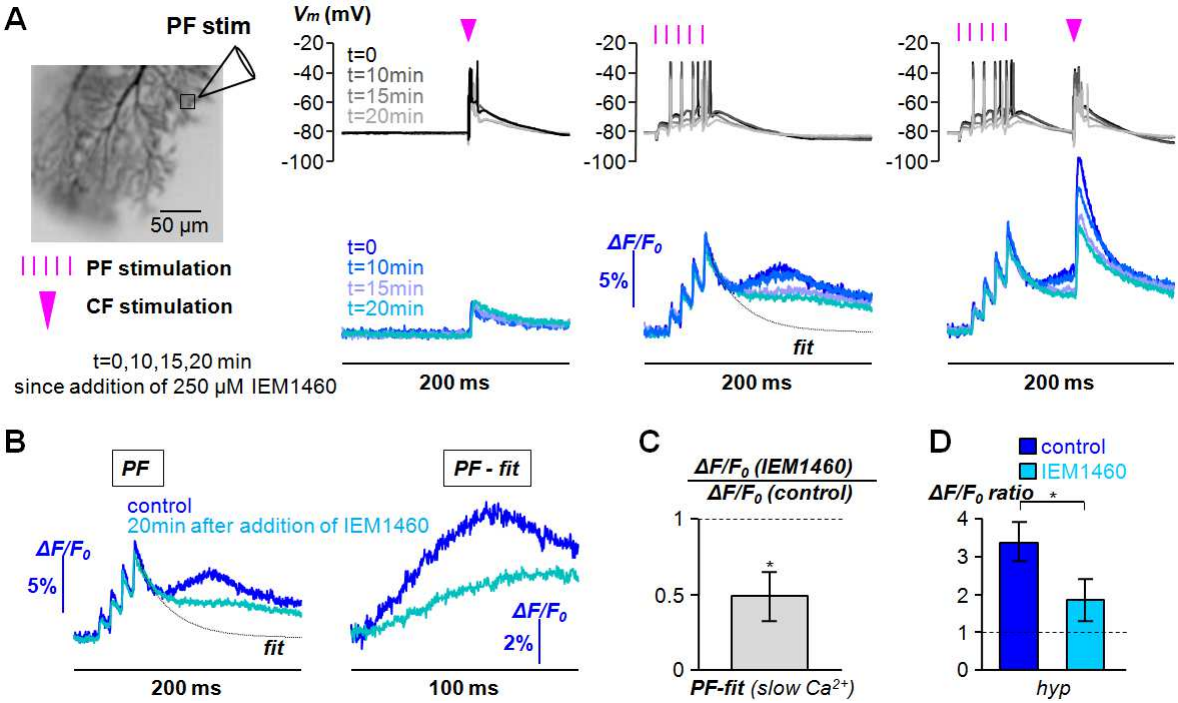
A
PF stim
50 µm
PF stimulation
CF stimulation
t=0,10,15,20 min
since addition of 250 µM IEM1460
Vm (mV)
-20
-40
-60
-80
-100
t=0
t=10min
t=15min
t=20min
ΔF/F0
5%
fit
200 ms

B
PF
PF - fit
control
20min after addition of IEM1460
ΔF/F0
5%
fit
200 ms
2%
100 ms
C
ΔF/F0 (IEM1460)
ΔF/F0 (control)
1
0.5
0
PF-fit (slow Ca2+)
D
control
IEM1460
ΔF/F0 ratio
*
4
3
2
1
0
hyp

Figure 10

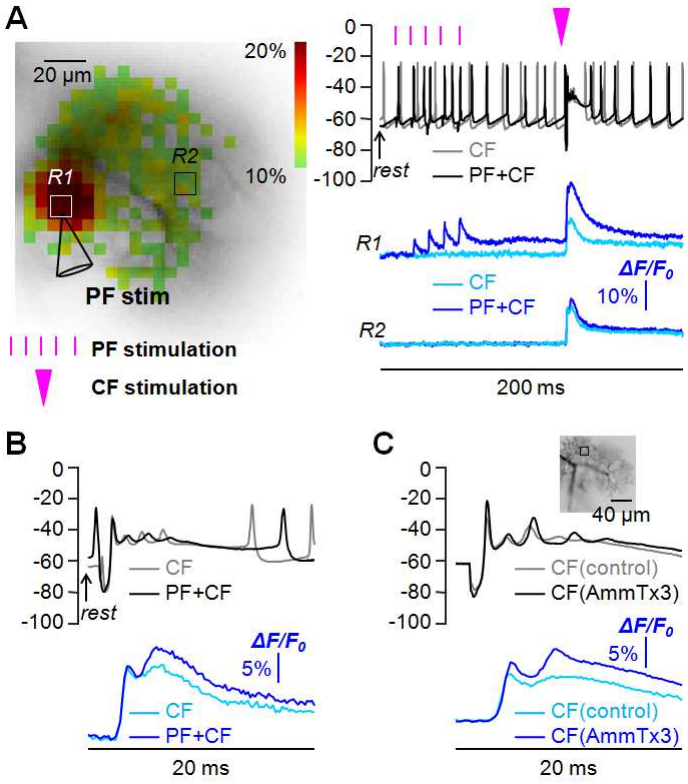
A
20 µm
20%
10%
R1
R2
PF stim
PF stimulation
CF stimulation
0
-20
-40
-60
-80
-100
rest
CF
PF+CF
R1
ΔF/F0
10%
R2
200 ms
B
rest
CF
PF+CF
ΔF/F0
5%
20 ms
C
40 µm
CF(control)
CF(AmmTx3)
ΔF/F0
5%
20 ms

Figure 11

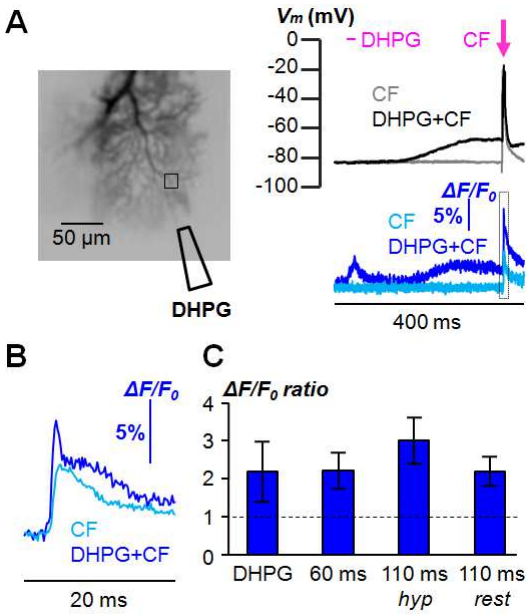
A
Vm (mV)
0
-20
-40
-60
-80
-100
- DHPG
CF
CF
DHPG+CF
ΔF/F0
5%
CF
DHPG+CF
50 µm
DHPG
400 ms
B
ΔF/F0
5%
CF
DHPG+CF
20 ms
C
ΔF/F0 ratio
4
3
2
1
0
DHPG
60 ms
110 ms
hyp
110 ms
rest

Figure 12

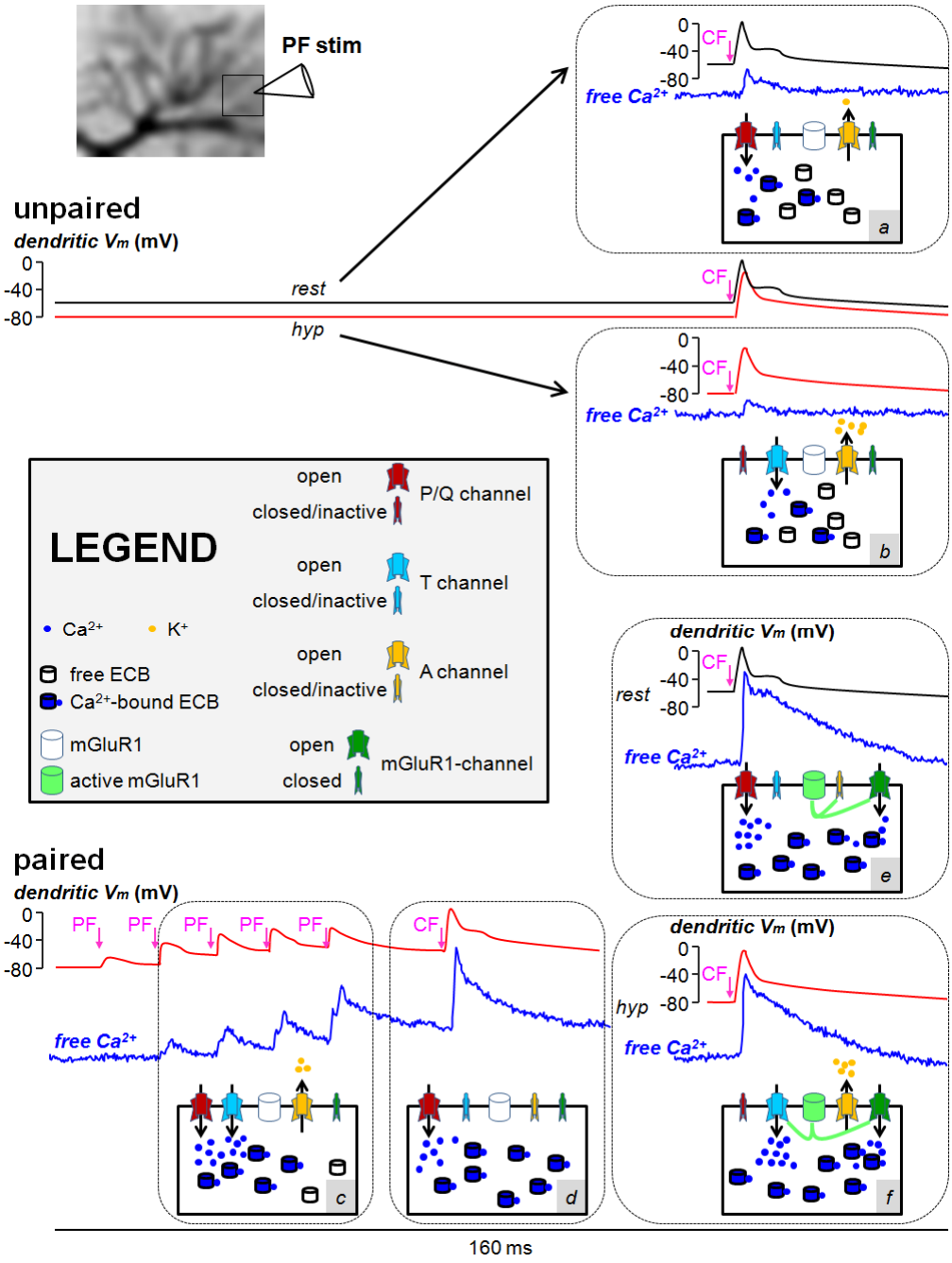
PF stim
unpaired
dendritic Vm (mV)
0
-40
-80
rest
hyp
CF
free Ca2+
a
b
LEGEND
open
closed/inactive
P/Q channel
T channel
A channel
Ca2+
K+
free ECB
Ca2+-bound ECB
mGluR1
active mGluR1
mGluR1-channel
closed
dendritic Vm (mV)
e
paired
PF
c
d
f
160 ms

Figure 13